DTIC FILE COPY

④

David Taylor Research Center

Bethesda, MD 20084-5000

Ambient Free Surface Wave Modification by a Submerged Vortex Pair

by
Scott Fish

Dissertation submitted to the Faculty of the Graduate School of the
University of Maryland in partial fulfillment of the requirements
for the degree of Doctor of Philosophy (1989).

DTIC
ELECTE
MAR 26 1990
S E D

90 03 23 067

MAJOR DTRC TECHNICAL COMPONENTS

CODE 011 DIRECTOR OF TECHNOLOGY, PLANS AND ASSESSMENT

12 SHIP SYSTEMS INTEGRATION DEPARTMENT

14 SHIP ELECTROMAGNETIC SIGNATURES DEPARTMENT

15 SHIP HYDROMECHANICS DEPARTMENT

16 AVIATION DEPARTMENT

17 SHIP STRUCTURES AND PROTECTION DEPARTMENT

18 COMPUTATION, MATHEMATICS & LOGISTICS DEPARTMENT

19 SHIP ACOUSTICS DEPARTMENT

27 PROPULSION AND AUXILIARY SYSTEMS DEPARTMENT

28 SHIP MATERIALS ENGINEERING DEPARTMENT

DTRC ISSUES THREE TYPES OF REPORTS:

1. **DTRC reports, a formal series,** contain information of permanent technical value. They carry a consecutive numerical identification regardless of their classification or the originating department.

2. **Departmental reports, a semiformal series,** contain information of a preliminary, temporary, or proprietary nature or of limited interest or significance. They carry a departmental alphanumerical identification

3. **Technical memoranda, an informal series,** contain technical documentation of limited use and interest. They are primarily working papers intended for internal use. They carry an identifying number which indicates their type and the numerical code of the originating department. Any distribution outside DTRC must be approved by the head of the originating department on a case-by-case basis.

REPORT DOCUMENTATION PAGE

1a. REPORT SECURITY CLASSIFICATION UNCLASSIFIED	1b. RESTRICTIVE MARKINGS
2a. SECURITY CLASSIFICATION AUTHORITY	3. DISTRIBUTION/AVAILABILITY OF REPORT
2b. DECLASSIFICATION/DOWNGRADING SCHEDULE	Approved for public release; distribution is unlimited

4. PERFORMING ORGANIZATION REPORT NUMBER(S) DTRC–90/004	5. MONITORING ORGANIZATION REPORT NUMBER(S)

6a. NAME OF PERFORMING ORGANIZATION David Taylor Research Center	6b. OFFICE SYMBOL (If applicable) Code 1543	7a. NAME OF MONITORING ORGANIZATION
6c. ADDRESS (City, State, and ZIP Code) Bethesda, MD 20084–5000		7b. ADDRESS (City, State, and ZIP Code)

8a. NAME OF FUNDING/SPONSORING ORGANIZATION	8b. OFFICE SYMBOL (If applicable)	8. PROCUREMENT INSTRUMENT IDENTIFICATION NUMBER

8c. ADDRESS (City, State, and ZIP Code)	10. SOURCE OF FUNDING NUMBERS

PROGRAM ELEMENT NO.	PROJECT NO.	TASK NO.	WORK UNIT ACCESSION NO.
61152N		ZR0230101	DN507319

11. TITLE (Include Security Classification)

AMBIENT FREE SURFACE WAVE MODIFICATION BY A SUBMERGED VORTEX PAIR

12. PERSONAL AUTHOR(S)
Fish, Scott

13a. TYPE OF REPORT Final	13b. TIME COVERED FROM_____ TO_____	14. DATE OF REPORT (YEAR, MONTH, DAY) 1990, February	15. PAGE COUNT 98

17. COSATI CODES			18. SUBJECT TERMS (Continue on reverse if necessary and identify by block number)
FIELD	GROUP	SUB–GROUP	Hydrodynamics ... ...
			Ships, Naval ... Free ... ...
			Vortices, Radar ... ...

19. ABSTRACT (Continue on reverse if necessary and identify by block number)

This research examines how free surface gravity waves travelling over a fluid are modified by the presence of a submerged pair of vortex singularities. The understanding of vortex flows near a free surface has become a major goal in the hydrodynamics community over the last decade due to its possible importance in determining the influence of vortical ship wakes on radar images of the ocean surface, a theory for vortical influence on ambient free surface waves has not been addressed. The inclusion of ambient surface waves is of fundamental importance in understanding the ship wake images observed under real ocean conditions. The first steps in uncovering the subtleties of the ambient free surface wave modification by submerged vortices are taken by concentrating on three questions. First, what is the important physical mechanism of influence of the vortex on free surface ambient waves? Second, in formulating a typical vortex model of the flow involving a rising pair, what parameters are significant in determing the form of the ambient wave modification? And finally, how can this information be useful in the practical problem of radar imaging of ship wakes? Careful analytic analysis of the free surface boundary conditions will show that the induced surface current generated by the vortices provides the physical mechanism of ambient wave modification. A numerical model is described which is utilized to determine the relative importance of parameters derived in the analytic analysis on this physical mechanism. In addition, spectral analysis is performed to highlight the use of simulation results in evaluation of conditions applicable to the problem of radar remote sensing of ship wakes.

20. DISTRIBUTION/AVAILABILITY OF ABSTRACT ☐ UNCLASSIFIED/UNLIMITED ☒ SAME AS RPT ☐ DTIC USERS	21. ABSTRACT SECURITY CLASSIFICATION UNCLASSIFIED
22a. NAME OF RESPONSIBLE INDIVIDUAL Scott Fish	22b. TELEPHONE (Include Area Code) (202) 227–1473 — 22c. OFFICE SYMBOL Code 1543

DD FORM 1473, JUN 86   Previous editions are obsolete.

PREFACE

This report presents the contents of a Ph.D. dissertation submitted to the University of Maryland Mechanical Engineering Department in the Fall of 1989. The faculty advisor for this work, and the person to whom the author extends much thanks, is Dr. Christian von Kerczek. The title of the dissertation is Ambient Free Surface Wave Modification By A Submerged Vortex Pair. The work was sponsored by the Independent Research (IR) Program Funded by ONT and administered by DTRC. In addition to this research funding, the Ship Hydromechanics Department at DTRC sponsored the author for nine months of Extended Term Training to complete course work, comprehensive examinations, and the background research for this study. The author wishes to acknowledge the contributions of both of these sources, without which this work might not have been completed.

Only cosmetic editing of the original dissertation has been performed here for closer conformity to DTRC report format. The appendices of the original dissertation have been omitted here for brevity. The reader is referred in the text where appropriate to the specific appendix containing additional information.

Finally, the author would like to thank Dr. Edwin Rood, whose supervision, encouragement, and technical guidance in the initial stages of the work provided the catalyst necessary for undertaking such an extensive research project.

Scott Fish

𝑋

A-1

iii

THIS PAGE INTENTIONALLY LEFT BLANK

CONTENTS

FIGURES

ABSTRACT

This research examines how free surface gravity waves travelling over a fluid are modified by the presence of a submerged pair of vortex singularities. The understanding of vortex flows near a free surface has become a major goal in the hydrodynamics community over the last decade due to its possible importance in determining the influence of vortical ship wakes on radar images of the ocean surface. Although much research has concentrated on studying vortices near a still free surface, a theory for vortical influence on ambient free surface waves has not been addressed. The inclusion of ambient surface waves is of fundamental importance in understanding the ship wake images observed under real ocean conditions. The first steps in uncovering the subtleties of the ambient free surface wave modification by submerged vortices are taken by concentrating on three questions. First, what is the important physical mechanism of influence of the vortex on free surface ambient waves? Second, in formulating a typical vortex model of the flow involving a rising pair, what parameters are significant in determining the form of the ambient wave modification? And finally, how can this information be useful in the practical problem of radar imaging of ship wakes? Careful analytic analysis of the free surface boundary conditions will show that the induced surface current generated by the vortices provides the physical mechanism of ambient wave modification. A numerical model is described which is utilized to determine the relative importance of parameters derived in the analytic analysis on this physical mechanism. In addition, spectral analysis is performed to highlight the use of simulation results in evaluation of conditions applicable to the problem of radar remote sensing of ship wakes.

ADMINISTRATIVE INFORMATION

CHAPTER 1 - INTRODUCTION

Research interest in the behaviour of vortex structures near a free surface has recently been revived by the detection of dark regions in radar images of the sea surface. The significance of these long narrow dark streaks is their coincidence with the centerline wake regions of ships travelling on the sea surface at the time of radar exposure. For this reason, they are generally referred to as dark *centerlines*. An example of the dark centerline, observed primarily on synthetic aperture radar (SAR), is shown in Fig 1a. The ship in this example is located at the intersection of the angled Kelvin wake lines as shown diagrammatically in Fig 1b. Other examples and details on the radar operation and image processing can be found in Lyden et al.[4] and Peltzer et al.[5] Although the cause of the dark centerlines is not well understood, there is widespread agreement that the lower energy radar return in this region is a result of the elimination of surface waves normally responsible for constructive interference in reflection of the radar signal. Constructive interference occurs when the component of the surface wavenumber vector in the "look" direction of the radar satisfies the following expression (Wright[6]):

$$k_w = 2 k_r \sin(\theta)$$

where: $k_w = 2\pi/\lambda_w$ = surface wavenumber

$k_r = 2\pi/\lambda_r$ = radar wavenumber

λ = wavelength

θ = vertical incidence angle of the radar (normal to the free

surface: $\theta = 0°$)

These waves, termed Bragg Scattering Waves, are typically wind generated, and form the background signal return level in SAR images. Dark centerlines in the radar images of moving ships at sea suggest the reduction or elimination of these Bragg Waves in the ship wake. This process has been suggested by some to be caused by, among other things, the turbulent ship wake generated by the ship. Measurements by Lindenmuth and Fry[8] and calculations by Griffin et al.[6] of the mean and rms velocity components behind a $1/20^{th}$ scale twin screw ship model indicate that the mean turbulent energy in the ship's wake dies out over much shorter distances than the obse.ved dark centerline. This has lead to the belief that the ship generated turbulence, or mean wake currents, play only a minor role in the production of the dark centerline. Observations by Fish and Blanton[4] suggest that the turbulent energy in the wake may be contained in large scale vortical structures which are widely dispersed far downstream in the ship wake. Under these conditions, the highly intermittent concentrations of vorticity may therefore not be accounted for in the previous time averaged measurements and computations. The question of the importance of vortical wakes on the dark surface centerline consequently remains unanswered. Other theories explaining the damping of ambient waves involve the redistribution of surfactants by mean vortex induced currents in the ship wake. The redistribution process is therefore governed by turbulent vortical wake influences on the surface. Regardless of whether this vorticity is generated by bow and/or stern wave breaking, propeller wash, or hull generated vorticity, the process occurs in the presence of ambient surface waves. These issues indicate a need for understanding the influence of submerged vortices on ambient surface waves.

In order to comprehend how the ship's wake interacts with the surface, researchers have constructed simple wake models. The most common vortical wake model used in examining the interaction with the free surface is a counter-rotating vortex pair. This model is illustrated in Fig 2. The choice of this model is two-fold. First, the vortex pair may be used as a crude model of the wake of a ship with either strong bilge vortices or twin outboard rotating propellers. Each vortex in the latter case represents the swirling flow generated by a propeller. These vortices are allowed to approach the surface with their mutually induced velocity. The vortex pair is also one of the simplest configurations for study and can be utilized as a building block towards understanding the much more complicated turbulent flow interaction with the free surface.

Prior studies of vortex-free surface interactions focused on the dynamics of an initially flat free surface under the influence of a relatively strong vortex pair. This problem is not directly relevant to the SAR imaging problem, however, due to the neglect of ambient waves responsible for the scattering of radar radiation. What is important is the modification of the ambient Bragg Scattering Waves by vortices of relatively weak strength. The terms "strong" and "weak" here refer to the vortex/(free surface) strengths characterized by a nondimensional parameter refered to as the Froude number. Differentiating between high and low values of the Froude number determines whether linearized boundary conditions can be used to model the free surface evolution. Because weak vortices generate small vertical surface deflections, and no wave breaking phenomena, it will be shown that linearization can maintain accuracy while providing greater insight into the

3

physics of the flow. Linearization of the free surface also allows simulation of simple monochromatic ambient waves without introducing second order self imposed profile modification. The alteration of these simple waveforms by submerged vortices can therefore only be identified under linearized conditions. Because Bragg wa ᵤs for typical radar wavelengths are much shorter than the depth of the modelled wake vortices, their influence on the vortex paths is negligible and will be ignored in this study. The resulting paths of the vortex pair will correspond to the paths for a still free surface. The analytic derivation of an alternate form of linearization under the above stated conditions gives insight into the dominant physical mechanism responsible for ambient wave modification in regions near submerged free vortices. Free in this context pertains to conditions of self induced motions of the vortices. The motivation for use of linearized theory is based primarily on the ability to simulate simple sinusoidal ambient waves in the final sections of the research. The justification for use of linearized theory will be given in chapters 2 and 3.

Simulations of the two dimensional vortex pair near a free surface with monochromatic ambient waves are used here to determine which parameters of the governing equations are dominant. It will be shown that the Froude number of the vortices and their initial positions play the most important roles in inducing surface currents. As the Froude number is increased, the vortex induced surface currents become stronger, resulting in greater compression of incoming ambient waves. The separation distance of the vortex pair manifests itself in the size of the disturbed surface region. Other parameters such as the ambient wave steepness and relative phase resulting from the analytic study as independent

quantities, play secondary roles, as might be expected by a linearized examination.

In addition, spectral analysis will be used in a form which extracts characteristics in the surface similar to the radar imaging process. This analysis will show that submerged vortices can give images with darker center regions where the ambient waves undergo the modification. This analysis will be performed on a vortex pair with parameters derived from typical ship operating characteristics.
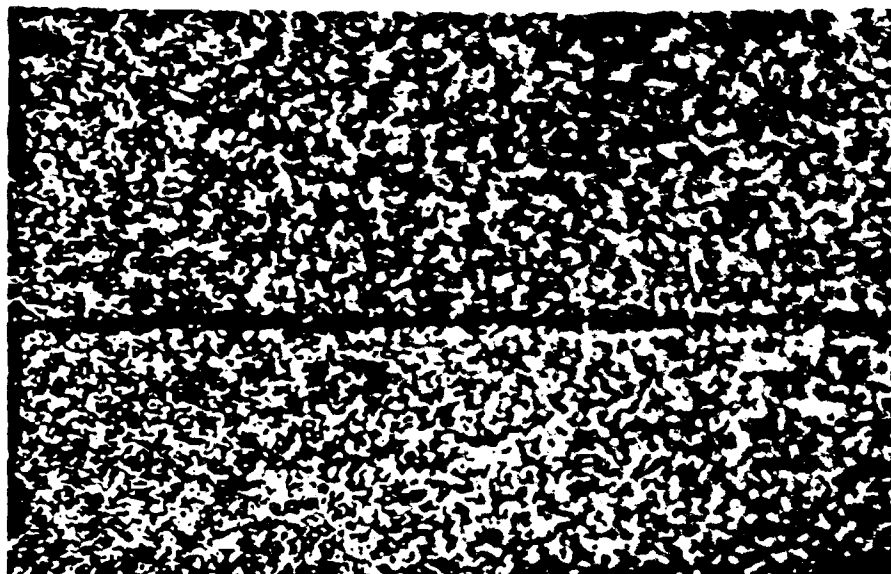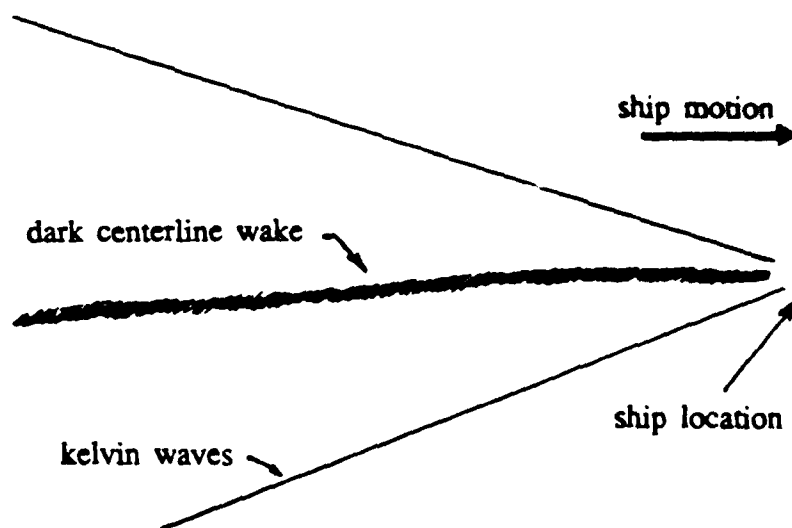
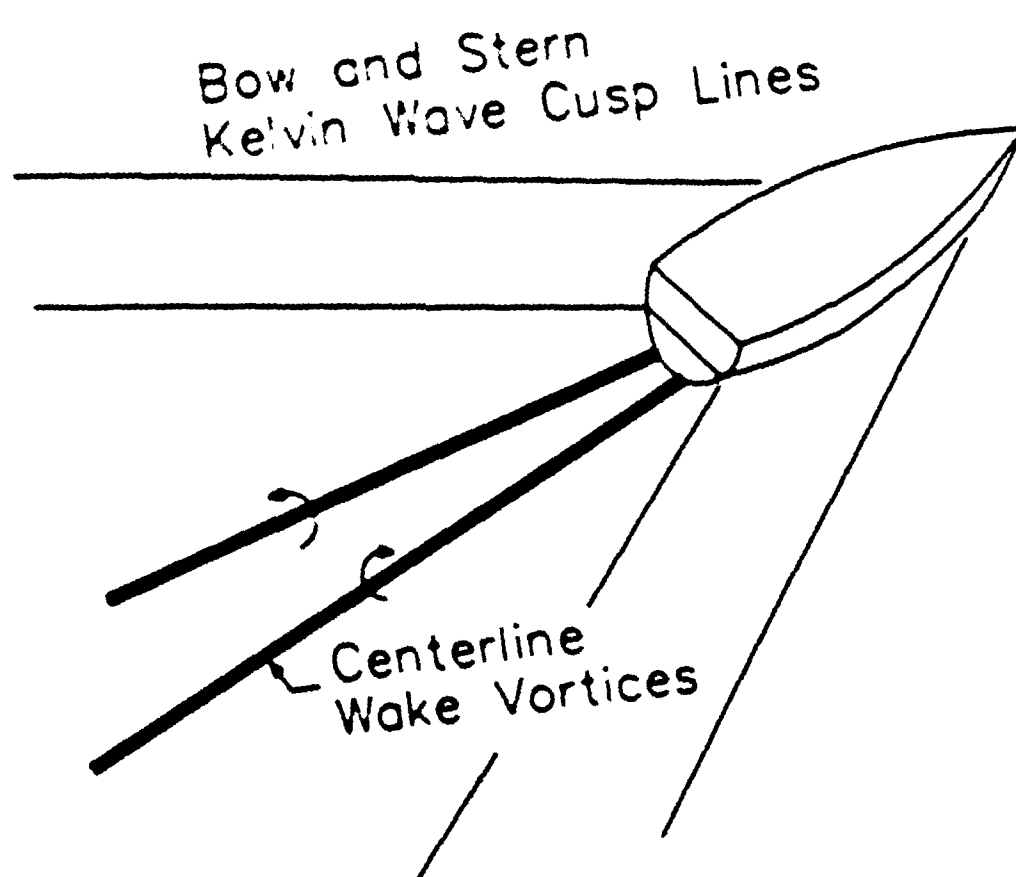Figure 1a - Example SAR Image of Ship Wake

Figure 1b - SAR Image Diagram

6

Bow and Stern
Kelvin Wave Cusp Lines

Centerline
Wake Vortices

Figure 2 - Ship Wake Model

7

CHAPTER 2 - BACKGROUND RESEARCH

Experimental realizations of the rising vortex pair model with a free surface were first carried out by Sarpkaya and Henderson[14] and Sarpkaya[15] using a submerged lifting surface. These studies showed two types of surface signature of the trailing vortices which were termed "scars" and "striations." "Scars" in this sense refer to longitudinal depressions in the free surface roughly aligned and positioned just outboard of each vortex. Scars begin appearing when the vortices are within one initial separation distance from the free surface. "Striations" are transversely aligned surface deformations which appear when the vortex pair are roughly one half their initial separation distance from the surface. Willmarth et.al.[22] have recently carried out experiments using flaps to generate two dimensional (2D) vortex pairs and observe their impinging on an initially still free surface. Two dimensional computations (also in Willmarth et.al.[22]) have been carried out showing good agreement with the experiments until the point of transition of the vortices to a turbulent state. Figure 3 illustrates this 2D vortex pair configuration.

Several numerical studies of this 2D vortex pair near a free surface have been carried out by Marcus[10], Sarpkaya et al.[16], Telste[20], and Tryggvasson[19]. All of these studies were conducted using nonlinear free surface boundary conditions and potential flow. The free surface is still and flat when the vortices are initialized. These studies show how vortex pairs with high strength rise towards the surface under self induced velocities and generate an upward bulge in the free surface in the central region with depressions on the outer edges. Under conditions of very high vortex strength, they have shown that the vortex pair

8

may actually rise through the initial surface location pushing a plume of fluid up through the center. Telste[20] also shows that for small Froude numbers ($F = \Gamma/(gS^3)^{1/2}$), the vortex path deviates very little from the rigid surface condition, and that the surface disturbances are both small, and localized to the region of the vortex. Trygvasson (1988) has also simulated the nonlinear free surface deformation for a pair of deformable vortex *blobs*. *Blobs* are models of a vortex structure composed of distributed vorticity in a finite region. The flow is computed using potential theory however and the vorticity distribution is discretized into vortex singularities. The surface deformations at low Froude numbers are insensitive to the detailed modelling of the vortex provided the *blob* size is small compared to the depth of the vortex.

For cases in which the vortex disturbance to the surface is weak in some sense, Wehausen and Laitone[21] give an exact solution for a linearized free surface following the classical assumptions used for surface wave theory. Both Marcus[10] and the author have exercised numerical evaluation of this solution (a double integral representing the Green's Function over the surface in time) over short time periods. The author has derived an alternate form of the classical solution (Wehausen and Laitone[21]), given in Appendix A of Fish[3], particularly suited for conditions of shallow vortices. However, both classical formulations, have been found by the author to be inadequate under conditions of self-induced motion of the vortices. This deficiency lies in an improper zero[th] order condition around which the linearization is performed, and is described in further detail in the next section.

9

Recent viscous flow simulations of the vortex pair approaching an initially still free surface have been carried out for laminar conditions including nonlinear free surface boundary conditions by Ohring and Lugt[12]. The current limitation of low Reynolds number of these calculations prevent them however from simulating flows of the typical ship scale. In addition, inclusion of surface waves, with their intrinsically large Reynolds numbers, still appears to be only a long range goal in their work.

Studies of wave modification by steady currents have also been pursued in recent years. Important differences exist however between these works and the present study. Cooper[2] and Griffin et al.[6] used conservation of wave action to examine the modification of short waves by surface current patterns. The surface current model used consisted of an axial velocity defect simulating the wake of a ship. Transverse currents were assumed negligible as were vertical current gradients. The orientation of the vortices as shown in Fig 2 generate transverse currents, and allow vertical current gradients as defined by the flowfield of the vortex pair. The most important difference, however, is the allowance of significant transverse current gradients in the direction of wave propagation. As will be found later, this condition, in conjunction with the short time scales of flow evolution for moderate vortex strengths, prevents the use of wave action conservation theory. Surface wave modification by vertical current gradients have been studied by Simmen and Saffman[17] and by Teles Da Silva and Peregrine[18] (1988). These studies concentrated on steady state alterations of deep and shallow water waves, respectively, by a linear vertical current gradient. A particularly important result of these works is the finding that the kinetic and

potential energies of the modified wave are unequal, suggesting that wave energy spectra calculated from surface height measurements may be inaccurate when current gradients are present. Recent measurements by Fry and Huang[5] of the modification of surface waves by submerged turbulence and a rising (somewhat two-dimensional) jet showed that modification was present, but give no details. In the present work, the transient response of the ambient waves will be examined rather than the steady state condition.

In order to address the specific flow conditions observed behind real ships, this research takes the first step in understanding the flow interaction between submerged vorticity and an ambient surface wave field. The influence of submerged vortex singularities on ambient surface waves will be characterized by numerically simulating the transient flow of an impulsively started vortex pair below an ambient wave field. Figure 4 shows a diagram of the flow being examined. Both experimental observations and numerical calculations indicate that vortex pairs of practical interest in the influence of the dark radar return regions of the wake are of relatively low Froude number. One expects therefore that a linearized free surface boundary condition can be used to sustain a simple monochromatic ambient wave for modification. The classical linearizations used by previous researchers however contain no analytical means of interaction between the vortices and the ambient waves. The solutions are simple superpositions of the ambient wave profile with the surface solutions corresponding to the initially still free surface. A new method of linearization must be developed to include interaction terms in the boundary conditions between the vortices and the ambient waves. This method is derived by

11

examining the physical mechanism of the interaction, and developing the proper choice of zeroth order solution around which to linearize. The resulting interaction theory is described in the next section.
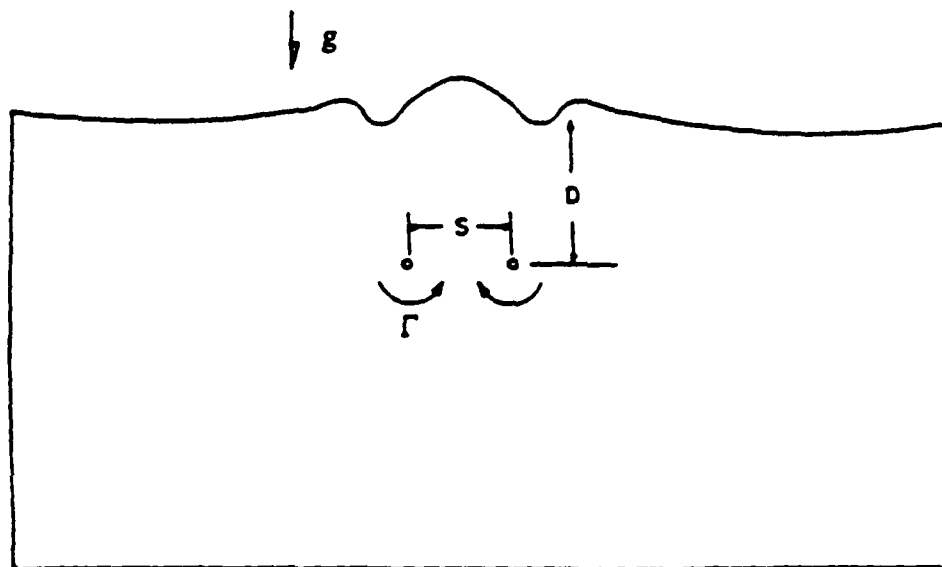
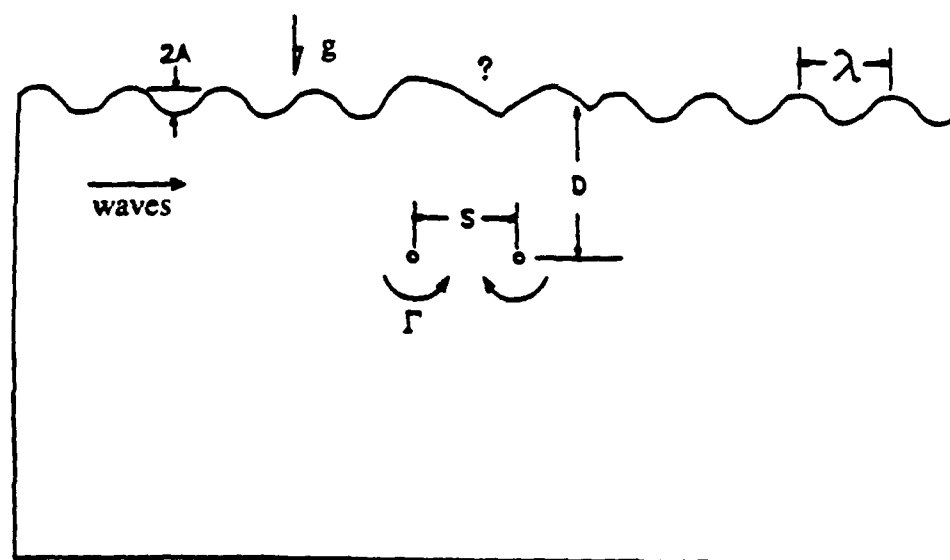Figure 3 - Typical Vortex/Free Surface Problem

Figure 4 - Ambient Wave Modification by Submerged Vortices

13

CHAPTER 3 - PHYSICAL MECHANISM FROM NEW LINEARIZATION

The development of a theory illuminating the physical mechanism responsible for ambient surface wave modification starts with examination of the flow equations. Free surface flows with waves are typically of such high Reynolds number that the flow can be considered inviscid (Newman[11]). The induced velocities in the vortex/free surface flows of concern here are sufficiently small that compressibility effects can also be ignored (Newman[11]). A two dimensional (2D) domain will be used here primarily for its simplicity in handling the quasi-2D vortex pair ship wake model described in the introduction and illustrated in Fig 2. The quasi-2D modelling assumption is that the velocity gradients along the axis of the ship are small and that a 2D flow realization in a plane normal to the ship axis may be integrated in time and stacked in space using the constant ship speed to represent the three dimensional problem.

The ambient waves are propagated from the side of the 2D domain as shown in Fig 4. These waves represent ambient waves moving transverse to the ship track. Because of the quasi-2D nature of the ship wake model, modelling waves propagating in directions much different from this lateral condition should not be assumed practical.

The free surface boundary conditions are being linearized for two reasons. The first reason for linearizing the free surface is to allow stable solutions for the propagation of sinusoidal ambient waves in the absence of the vortices. Vortex induced modifications to this simple ambient wave form may then be easily detected and quantified using spectral analysis. The second reason for linearizing the free surface boundary conditions is to obtain simpler equations to solve. If

14

the linearization is valid, the equations will reflect the correct physics for the problem and will be easier to interpret.

This section will develop a new form of linearized boundary conditions using a more appropriate form of zeroth order solution than that used in classical free surface flow linearizations. This new linearization method, which will be refered to as the alternate linearized method (ALM), properly accounts for the interaction of submerged vortices moving under self induction with the free surface. Once the ALM is developed, comparisons are made with both the classical linear and the fully nonlinear theories of vortex interaction with a free surface. Additional insight and justification for the ALM will be given in this comparison. The physical mechanism responsible for the modification of ambient surface waves also becomes apparent in this comparative analysis.

All of the equations used in this study are nondimensionalized. Subscripted notation will also be used to signify the partial differential operator unless otherwise noted.

For example: $\phi_y = \partial\phi/\partial y$

3.1 BOUNDARY CONDITION DEVELOPMENT

Under the above described conditions, the flow can be represented using a velocity potential, the gradient of which gives the fluid velocity field. This velocity potential must be analytic in the fluid domain, and therefore satisfy Laplace's equation (Newman[11]):

$$\phi_{xx} + \phi_{yy} = 0 \qquad \text{(for two dimensional flow)}$$

The singular representation of a 2D point vortex must therefore be removed from the fluid domain by properly choosing the boundary of the flow to include a vanishingly small enclosure of this singularity.

Additional equations describing the flow are obtained by enforcing boundary conditions at the edges of the simulation domain. The fully nonlinear boundary conditions at the free surface are given by (Newman[11]):

Dynamic Boundary Condition: (on $y = \eta$)

$$\phi_t(x,\eta,t) + \frac{\phi_x^2(x,\eta,t) + \phi_y^2(x,\eta,t)}{2} + \frac{\eta(x,t)}{F^2} = 0 \qquad (1a)$$

Kinematic Boundary Condition: (on $y = \eta$)

$$\frac{D}{Dt}(y-\eta) = \phi_y(x,\eta,t) - \eta_t(x,t) - \phi_x(x,\eta,t)\,\eta_x(x,t) = 0 \qquad (1b)$$

where: $F = \dfrac{\Gamma}{(g\,D^3)^{1/2}} \qquad \phi = \dfrac{\phi'}{\Gamma} \quad \eta = \dfrac{\eta'}{D} \quad t = \dfrac{t'\Gamma}{D^2}$

D = characteristic length scale (usually vortex depth)
Γ = vortex circulation
g = gravitational acceleration
ϕ = velocity potential
η = free surface elevation above still surface level
(note: ' represents dimensional quantity)

Vortex Velocity Condition:

V = induced velocity from other vortex and images in free surface

These equations, in addition to Laplace's equation in the fluid domain must be satisfied for the flow simulation. The linearization process is applied to the free surface boundary conditions for the purpose of simplifying the mathematics and numerical flow simulation model while retaining the dominant features of the flow.

The first step in a linearization procedure is the choosing of both the state or condition around which one wants to linearize, and the small perturbation parameter. The linearized solution will therefore be composed of this baseline solution plus a power series of solutions in the small perturbation parameter

$$\phi = \phi_0 + \varepsilon\phi_1 + \varepsilon^2\phi_2 + \cdots \qquad (2a)$$

$$\eta = \eta_0 + \varepsilon\eta_1 + \varepsilon^2\eta_2 + \cdots \qquad (2b)$$

Each ϕ_i must satisfy Laplace's equation $\nabla^2\phi_i = 0$ in the fluid domain. The choice of baseline solution around which to linearize is governed by the desire to minimize the value of the perturbation series, hence the desire to use the closest known approximate solution to the problem being addressed

In the classical linearization, one assumes that Γ is the small perturbation parameter. This implies that the disturbances in ϕ and η are small. The base state, or zero[a] order solution, therefore is $\phi_0 = \eta_0 = 0$ everywhere. The derivation of the resulting classical linearized boundary conditions can be found in Appendix B of Fish'. The resulting classical linearized method (CLM) results in linearized free surface boundary conditions given by (note: $\phi = \phi_0 + \varepsilon\phi_1$, $\eta = \eta_0 + \varepsilon\eta_1$)

$$\text{Dynamic:} \quad \phi_t + \eta/\varepsilon = 0 \qquad (\text{on } y = 0) \qquad (3a)$$

$$\text{Kinematic:} \quad -\phi_y + \eta_t = 0 \qquad (\text{on } y = 0) \qquad (3b)$$

In the CLM ther are two distinct governing flow parameters. One of these, the speed of the vortex, is assumed to be of order one; and the other, the Froude number based on Γ is be assumed to be of order ε. Further discussion of these parameters and their implications will be made in the section "Comparison of the Methods."

17

This chapter shows that a new, more representative solution may be used as the baseline, or 0th order solution to provide greater insight into the interaction of vortices with a free surface.

3.1.1 Alternate Linearization Method (ALM)

The ALM is developed around a more meaningful 0th order solution for flows with submerged vortex singularities of low Froude number (F). In this case the baseline solution is the resulting flow in the limit as F, the small perturbation parameter goes to zero. This condition corresponds to having the gravitational acceleration so much greater than the vortex strength divided by the vortex depth, that the surface boundary conditions approach those of a rigid wall. The zeroth order solution therefore corresponds the rigid wall condition, and is formulated as the sum of the potential of the vortex and its image above the surface: (in dimensional form)

$$\phi_0 = \Gamma/2\pi i \left[\ln(z-c) - \ln(z-c') \right]$$

Here, $z = x + iy$ and c is the complex location of the vortex below the rigid surface. The c' represents the complex conjugate or image of c when the rigid boundary is located at $y = 0$. The corresponding surface elevation for the rigid wall condition is, by definition, $\eta_0 = 0$. This can be confirmed by substitution of $F = 0$ into the Dynamic Boundary condition. The perturbation expansion parameter (ε) will represent the value of the Froude number squared for simplicity, so this method can be assumed valid only for small values of F^2.

Because the nonlinear boundary conditions are satisfied on the deflected surface elevation position, and in linearizing one would like to satisfy the boundary conditions on $y = 0$ ($\eta_0 = 0$), one must expand the boundary conditions (1) in a power series in η (an order ε quantity) for terms evaluated at $y = 0$. For example, take a single term from the dynamic boundary condition:

$$\phi_t(x,\eta,t) = \phi_t(x,0,t) + \eta \; \phi_{ty}(x,0,t) + \eta^2 \phi_{tyy}(x,0,t)/2 + \cdots$$

The resulting expanded boundary condition equations are shown below: (keeping only two terms in each Taylor series)

Dynamic: $\phi_t + \eta \; \phi_{ty} + 1/2 \left((\phi_x + \eta \; \phi_{xy})^2 + (\phi_y + \eta \; \phi_{yy})^2 \right) + \eta/\varepsilon = 0$ (4a)

Kinematic: $-\phi_y - \eta \; \phi_{yy} + \eta_t + \eta \; \eta_{ty} + (\phi_x + \eta \; \phi_{xy})(\eta_x + \eta \; \eta_{xy}) = 0$ (4b)

19

The ϕ and η expansions **(2)** are next substituted into the above equations to obtain the following expressions:

Dynamic:

$$(\phi_{0_t} + \epsilon\phi_{1_t} + \epsilon^2\phi_{2_t}) + (\epsilon\eta_1 + \epsilon^2\eta_2)(\phi_{0_{ty}} + \epsilon\phi_{1_{ty}} + \epsilon^2\phi_{2_{ty}}) +$$

$$0.5\left[(\phi_{0_x} + \epsilon\phi_{1_x} + \epsilon^2\phi_{2_x}) + (\epsilon\eta_1 + \epsilon^2\eta_2)(\phi_{0_{xy}} + \epsilon\phi_{1_{xy}} + \epsilon^2\phi_{2_{xy}})\right]^2 +$$

$$0.5\left[(\phi_{0_y} + \epsilon\phi_{1_y} + \epsilon^2\phi_{2_y}) + (\epsilon\eta_1 + \epsilon^2\eta_2)(\phi_{0_{yy}} + \epsilon\phi_{1_{yy}} + \epsilon^2\phi_{2_{yy}})\right]^2 +$$

$$(\epsilon\eta_1 + \epsilon^2\eta_2)/\epsilon = 0$$

Kinematic:

$$-(\phi_{0_y} + \epsilon\phi_{1_y} + \epsilon^2\phi_{2_y}) - (\epsilon\eta_1 + \epsilon^2\eta_2)(\phi_{0_{yy}} + \epsilon\phi_{1_{yy}} + \epsilon^2\phi_{2_{yy}}) + (\epsilon\eta_{1_t} + \epsilon^2\eta_{2_t}) +$$

$$(\epsilon\eta_1 + \epsilon^2\eta_2)(\epsilon\eta_{1_{ty}} + \epsilon^2\eta_{2_{ty}}) + (\phi_{0_x} + \epsilon\phi_{1_x} + \epsilon^2\phi_{2_x})(\epsilon\eta_{1_x} + \epsilon^2\eta_{2_x}) +$$

$$(\epsilon\eta_1 + \epsilon^2\eta_2)(\epsilon\eta_{1_x} + \epsilon^2\eta_{2_x})(\phi_{0_{xy}} + \epsilon\phi_{1_{xy}} + \epsilon^2\phi_{2_{xy}}) +$$

$$(\epsilon\eta_1 + \epsilon^2\eta_2)(\phi_{0_x} + \epsilon\phi_{1_x} + \epsilon^2\phi_{2_x})(\epsilon\eta_{1_{xy}} + \epsilon^2\eta_{2_{xy}}) +$$

$$(\epsilon\eta_1 + \epsilon^2\eta_2)(\phi_{0_{xy}} + \epsilon\phi_{1_{xy}} + \epsilon^2\phi_{2_{xy}})(\epsilon\eta_{1_{xy}} + \epsilon^2\eta_{2_{xy}}) = 0$$

These equations can then be broken down into sub-equations in each power of ε. The Dynamic Boundary condition is multiplied through by ε to remove the ε from the denominator of the last terms on the left hand side. The resulting equations may then be compared at equivalent powers of ε as follows:

<u>Dynamic:</u>

$$\varepsilon^0: \qquad \eta_0 = 0 \tag{5a}$$

$$\varepsilon^1: \qquad \phi_{0_t} + 0.5\,\phi_{0_x}^2 + \eta_1 = 0 \tag{5b}$$

$$\varepsilon^2: \qquad \phi_{1_t} + \phi_{0_x}\phi_{1_x} + \eta_2 = 0 \tag{5c}$$

$$\varepsilon^3: \qquad \phi_{2_t} + \eta_1\phi_{1_{ty}} + \phi_{0_x}\phi_{2_x} + 0.5\,\phi_{1_x}^2 + \eta_1\phi_{0_x}\phi_{1_{xy}} + \phi_{1_y}^2 + \eta_3 = 0 \tag{5d}$$

<u>Kinematic:</u>

$$\varepsilon^0: \qquad -\phi_{0_y} = 0 \tag{6a}$$

$$\varepsilon^1: \qquad -\phi_{1_y} + \eta_{1_t} + \phi_{0_x}\eta_{1_x} - \eta_1\phi_{0_{yy}} = 0 \tag{6b}$$

$$\varepsilon^2: \quad -\phi_{2_y} - \eta_1\phi_{1_{yy}} + \eta_{2_t} + \eta_1\eta_{1_{ty}} + \phi_{0_x}\eta_{2_x} + \phi_{1_x}\eta_{1_x} + \eta_1\phi_{0_x}\eta_{1_{xy}} - \eta_2\phi_{0_{yy}} = 0 \tag{6c}$$

The first order problem (Eq. 5b) shows that the 1ˢᵗ order free surface elevation can be computed as a by product of the known zeroth order potential. The known η_1 and ϕ_0 can then be substituted into the Laplace's equation and boundary condition 6b to determine ϕ_1. Known ϕ_0, ϕ_1, and η_1 may then be used in boundary condition 5c to determine η_2. This method of cycling through the boundary condtion equations of increasing order for more accurate solutions is a characteristic of quasi-steady problems. Solving the unsteaddy free surface problem by this method is extremely combersome, however. The prefered solution method is to solve the Laplace equation at an instant in time and

21

integrate this solution forward in time using the boundary conditions. This time integration method of solution is, in fact, required to properly incorporate interaction terms between the vortex induced velocities and the ambient waves.

By eliminating all terms of order ε^2 or greater, the following expressions are obtained:

Dynamic:

$$\phi_{0_t} + \varepsilon \, \phi_{1_t} + \phi_{0_x}^2/2 + \eta_1 = 0 \qquad\qquad (7a')$$

Kinematic:

$$-(\phi_{0_y} + \varepsilon \, \phi_{1_y}) + \varepsilon \, \eta_{1_t} + \varepsilon \, \phi_{0_x}\eta_{1_x} - \varepsilon \, \eta_1 \, \phi_{0_{yy}} = 0 \qquad\qquad (7b)$$

One can now obtain a solution of η to second order by adding terms from the left side of Eq. 5c, who's sum is zero, to the dynamic boundary condition 7a'. The resulting Dynamic boundary condition is given by:

Dynamic:

$$\phi_{0_t} + \varepsilon \, \phi_{1_t} + \phi_{0_x}^2/2 + \varepsilon \, \phi_{0_x}\phi_{1_x} + \eta_1 + \varepsilon \, \eta_2 = 0 \qquad\qquad (7a)$$

In order to compare these equations to Eq. 3 from the Classical Linearization Method (CLM), they should be rewritten in terms of the variables ϕ and η (where: $\phi = \phi_0 + \varepsilon\phi_1$ and $\eta = \varepsilon\eta_1 + \varepsilon^2\eta_2$, note: ϕ_0 is different in CLM from ALM). Several order ε^2 terms must be added to Eq. 7 for this rewriting. For example, $0.5 \, \phi_{1_x}^2$ is added to the dynamic boundary condition 7a, and ($\phi_{0_x}\eta_2 + \eta_2\phi_{0_{yy}}$) is added to the kinematic boundary condition 7b. This adding of higher order terms is legitimate as long as the final result is only considered accurate to the

original order: $\phi = \text{order}(\varepsilon)$, $\eta = \text{order}(\varepsilon^2)$. The following rewritten equations result:

Dynamic:
$$\phi_t + 0.5\ \phi_x^2 + \eta/\varepsilon = 0 \tag{8a}$$

Kinematic:
$$-\phi_y + \eta_t + \phi_0{}_x \eta_x - \eta\ \phi_0{}_{yy} = 0 \tag{8b}$$

3.1.2 Comparison of the Methods

The alternate linearized method (ALM) should now be compared with both the classical linearization method (CLM) and the nonlinear method to determine the flow conditions under which each of these methods produces the most accurate modelling. The examination starts with evaluation of the characteristic parameters of the flow being simulated. For a single vortex, a dimensional analysis of the flow indicates that two independent parameters can be defined as shown below:

$$F = \frac{\Gamma}{(g\ D^3)^{1/2}} \qquad G = \frac{V}{(g\ D)^{1/2}}$$

F represents the traditional Froude number based on the strength of both the vortex and the gravitational field, and a characteristic length scale such as the depth of submergence. This is the small parameter used in the ALM. As F increases the vortex exerts a greater influence on the free surface by a combination of:

       (a) strong vortex circulation strength

       (b) shallow submergence depth

       (c) weak gravitational acceleration strength

23

This parameter must be small for validation of either method, due to their assumptions that the surface disturbance is a small quantity.

The parameter G is an independent parameter relating the translational speed of the vortex, the gravitational strength, and a characteristic length scale. Note that nothing mathematically has yet been specified concerning the speed of the submerged vortex. The extra terms of the ALM boundary conditions should therefore be examined for varying G while keeping F small.

For large G, the physical problem involves a vortex which is moving at high speed/depth ratio. This is typical of moving lifting surfaces which are forced at a much higher velocity than that induced on the foil by the surrounding fluid. Under these conditions, the time derivative of the potential on the free surface may be much larger than the spatial derivative. Looking at Eq. 8, the additional terms have spatial derivatives of second order and can be assumed to be small compared with the time derivative and first order spatial derivative terms. This indicates that the CLM boundary conditions given by 3 are good approximations for high values of G.

If G is small, the spatial derivatives may be of the same order as the time derivatives and the additional terms given by the ALM boundary conditions may be significant. To estimate the significance of these extra terms for a "free" vortex, the following analysis is given. For small F, the velocity of the vortex can be approximated by the velocity induced on its position by its image vortex above the surface. This velocity can be expressed nondimensionally by $V = 1/(4\pi D)$. In order to have the additional term in the Dynamic boundary condition be of same order as the time derivative term we can change to a

24

constant velocity coordinate system moving with the vortex to express the time derivative term as: $\phi_t = V \phi_x$. Note that for small F, ϕ_x can be approximated by $1/(2\pi D)$ and V can be approximated by $1/(4\pi D)$. The resulting expressions for ϕ_t and $\phi_x^2/2$ are identical:

$$\phi_t = V \phi_x = 1/(8\pi^2 D^2) \qquad \phi_x^2/2 = 1/(8\pi^2 D^2)$$

The effect of neglecting the extra ALM terms in computation of low Froude number surface deflections with "free" vortices will be shown in the next section describing the interaction mechanism. Figure 9 will show the disagreement between the two methods of linearization and the erroneous prediction of an upward hump rather than a downward dip in the surface over the vortices.

The above discussion shows that under "free" vortex conditions and low values of Γ^2/gD^3, the extra terms given by the ALM contribute significantly to the calculation of the surface deformation. If one places an additional constraint on the flow by prescribing the way the vortex will move, then the originally independent G parameter becomes dependent on F through this constraint. This comparison shows that if the vortex moves as a "free" singularity, i.e., it moves with velocity prescribed by the gradient of the potential (excluding the local singularity) evaluated at its position, then G is small when F is small. Linearized modelling of free surface flows with submerged "free" vorticity should therefore apply the ALM instead of the CLM for accurate simulation of the flow.

3.2 INTERACTION MECHANISM - INDUCED SURFACE CURRENT

In order to evaluate the importance of the additional terms present in the ALM, a numerical simulation code was performed with and without these terms. The simulations involve both still and wavy free surfaces. The still surface cases are performed for comparison with nonlinear results obtained by Telste[20]. The wavy surface case is simply a sample of the many cases explored in the parametric study of the next section, and is used to highlight the influence of the terms representing the vortex induced surface current. Before describing these results however, a brief description of the numerical technique, known as the Boundary Integral Technique (BIT), is given. More detailed discussion of the BIT is given in Appendix C of Fish[3].

3.2.1 Numerical Simulation Method: (BIT)

The Boundary Integral Technique, or BIT, is a commonly used numerical method for potential flow study. The BIT conceptually splits the solution method into two distinct parts. The first part is the solution of Laplace's equation in the fluid domain given the distribution of either ϕ or ψ on the boundary. The second part of the solution is the extrapolation of new values of ϕ or ψ on the boundaries using the unsteady boundary conditions.

In addressing the first part of the BIT solution Cauchy's integral formula is applied to the fluid domain. Cauchy's Theorem states that a nonsingular function in a specified domain is completely defined by its values on the bounding surface through Cauchy's integral formula. The BIT is utilized in this study in the following manner. First, one constructs the complex potential $\beta(z,t) =$

26

$\phi(z,t)+i\psi(z,t)$ where $z = x+iy$. If β is analytic then Cauchy's integral formula states that

$$\oint_\Omega \frac{\beta}{z - z_0} \, dz = 0 \tag{7}$$

where: $\oint_\Omega$ is the closed contour integral along the boundary Ω and: z_0 is outside the boundary. Figure 5 shows that the boundary Ω is composed of both the free surface and all other boundaries. Since vortex singularities exist inside our boundary, infinitesimally small circular boundaries must be added around them. The practical implication of this is that the known complex potential due to each singularity must be subtracted from the total complex potential to obtain an analytic function. The resulting perturbation potential is solved using the BIT and added back to the singularity potentials to obtain new total potential values. β here will therefore refer to the analytic complex perturbation potential.

In the limit as z_0 approaches Ω from the outside, a small semi-circle may be formed in Ω at z_0 whose contribution to 7 can be extracted forming the following equation:

$$\int_\Omega \frac{\beta}{z-z_0} \, dz + i\alpha_0\beta(z_0,t) = 0$$

where: $\int_\Omega$ is a Cauchy principal value integral around Ω, and α_0 is the included angle between left and right Ω tangents at z_0.

One may discretise the contour into N panels for numerical integration of this equation evaluated at N z_0 positions on the boundary. The result is N equations and 2N unknowns corresponding to the ϕ and ψ values at the discrete boundary points. If one can prescribe values for either ϕ or ψ at each boundary

27

point, the missing component may be solved for. On the free surface, one may

prescribe a known initial distribution of ϕ. On all other boundaries ψ will be

prescribed. The common points between free surface and other boundaries will

therefore have both ϕ and ψ known. This results in N - 2 unknowns and one

may choose to solve either the real or imaginary part of Eq. 7. Fewer unknown

quantities are necessary if the real part is used on the z_0 points corresponding to

the free surface and the imaginary part is used on the z_0 points associated with

the other boundaries. The forms of these equations are given below. The

resulting N - 2 integral equations are approximated using trapezoidal spatial

summation and may be solved for the N - 2 unknowns by matrix inversion, the

details of which are given in Appendix C of Fish[3].

The resulting ϕ and ψ values represent equilibrium solutions to Laplace's

equation for a single time step. These values are numerically differentiated as

necessary using three point central differencing for substitution into the free

surface boundary conditions. The boundary conditions are used in a trapezoidal

time integration form as follows:

Kinematic: $\eta(t+\Delta t) = \eta(t) + \Delta t\, (\phi_y - \phi_0{}_x \eta_x + \eta\, \phi_0{}_{yy})$

Dynamic: $\phi(t+\Delta t) = \phi(t) + \Delta t\, (.5\phi_0{}_x^2 + \phi_0{}_x \phi_1{}_x + \eta/F)$

to advance the solution to the next time step. This time integration is actually

carried out in a predictor/corrector scheme for greater stability. The details of

this operation are also given in Appendix C of Fish[3].

Several special considerations in simulating free surface flows deserve

mentioning. The first is the handling of radiation conditions. Radiation

conditions typically prevent solutions which involve wave propagation into the flow domain from outside. Wave damping regions near the edges of the free surface have been used by some to prevent "reflections" of outgoing waves. Telste[20] gives an excellent example of this. Damping regions are not used in this research because of their detrimental effect on the ambient waves being simulated. Ambient wave reflections are minimized by prescribing boundary conditions at the edges of the free surface corresponding to the undisturbed ambient wave potential and stream function. The combination of this prescription of wave potential on the edges with an initial distribution of both wave potential and elevation at $t = 0$ provide the ambient wave energy needed in the simulation. The ambient wave model used here is a monochromatic sinusoidal deep water wave. Over the time periods simulated here, this technique proved adequate. The small amount of wave reflection caused by coupling of vortex potential with ambient wave potential on the edge of the free surface was small and appeared to have little influence on the main interaction region over the time scales simulated.

The computer code used in this research was essentially written from scratch in FORTRAN. The author used "canned" subroutines for performing the LU Decomposition of the geometric influence coefficients of the boundary in the Cauchy integral, and the numerical differentiation of variables for the free surface boundary condition solution.

3.2.2 Numerical Accuracy

The simulation program is evaluated for numerical error by simulating the known solution for linearized deep water waves with extremely small vortex strength. Zero vortex strength could not be simulated by virtue of the nondimensionalization scheme chosen for the boundary conditions. The reason for this is that coefficients in both the wavemaker boundary conditions and the dynamic free surface boundary condition contained vortex strength in the denominator. A check was therefore performed for $F = {}^1 e\text{-}5$ on a domain sized five ambient wavelengths in both depth and width. The vortices were located near the center of the domain, and moved little during the checkout time scale.

The numerical computations performed in the simulation can be divided into two phases. The first phase concentrated on the calculation of the Cauchy integral around the boundary. In order to test the accuracy of this portion, a deep water wave velocity potential (ϕ) was distributed over the boundary elements and the program was used to find the corresponding stream function (ψ). This test simulated the first step in the final program format, and contained no time stepping influence. An error could then be measured by comparing the calculated stream function and the exact analytic solution. The maximum error in this calculation occurred at the peaks and troughs of the waves, as suspected, where the magnitude of the second derivative of the potential is greatest. A logarithmic plot of this error versus the boundary element length is given in Fig 6. The slope of this plot was measured as 2.16. A slope of 2 corresponds to the theoretical error limit for use of the trapezoidal rule in evaluation of the Cauchy boundary integral. This shows that trapezoidal integration error is the

dominant numerical approximation in the calculations and could be reduced by implementing a higher order integration metho.'. The trapezoidal method of boundary integration was retained for this study due to its simplicity however, and a sufficiently fine boundary grid size was chosen to evaluate the dominant character of the vortex interaction.

The second phase of the calculations looked at the time stepping procedure. The velocity potential and free surface elevation were integrated forward in time using the free surface boundary conditions in a predictor/corrector method. In addition, numerical derivatives of the stream function, velocity potential and surface elevation must be calculated along the free surface for inclusion in the boundary condition equations. For stability reasons, a second order central difference scheme was used for derivative calculation except at the end points, where a second order one sided difference scheme was used. Numerical errors resulting from these calculations were tested by combining the time stepping with the Cauchy boundary integration in order to simulate the full form of the program. Again, a known deep water wave was input and allowed to propagate one wavelength before calculations were terminated. The calculated free surface profile after moving one wavelength was then compared to the exact solution. The errors found in the comparison were composed of both dissipation and dispersion components. These can be seen in Fig 7 which shows the surface elevation solution of a plane travelling wave using 16 grid points per wavelength. Over the time scale of one period of the wave, this case shows a 4.8% decrease in the mean wave amplitude, and a 1.7% oscillation in amplitude at a frequency roughly twice the wave frequency. This error is the manifestation of the Cauchy

31

boundary integration errors described above, the numerical differentiation errors in evaluation of the potential and elevation gradients on the free surface, and the time integration of the potential and elevation using the boundary condition equations. Figure 8 shows the influence of varying grid density on the magnitude of these errors. A resolution of 64 grid points per wavelength was chosen for all of the simulations shown in this report except the ship wake model. The domain size was maximized at this resolution to be 14 ambient wavelengths wide. This domain size was limited by the available core memory of the DTRC Cray XMP used for the simulations. Although larger memory sizes would allow greater size and accuracy in modelling the ship wake, the current size proved adequate for the purposes of this study. The decay over one wave period at this density was 0.25%, and the oscillation amplitude was approximately 0.4%.

3.2.3 Comparison With Nonlinear Method

Before delving into the complex simulations involving ambient waves, simulations were run for the vortex pair without ambient waves. The purpose of this test was to compare simulation output with independent results obtained by Telste[20] using a fully nonlinear free surface method. From these comparisons, some insight into the limitations of the linearized method could be determined, and considered in interpretation of the more complicated problem involving ambient wave modification.

Two Froude number cases were used for comparison. These corresponded to the "low" and "moderate" vortex strength cases presented by Telste. The

"high" Froude number case was not simulated because nonlinear vortex trajectories in this case were significantly influenced by the free surface and did not closely follow the path expressly used in the linearized method. This limitation in the linear theory may be partially overcome at moderate Froude number values by utilizing Cauchy's integral theorem to compute the induced velocity at the current vortex position from potentials on all boundaries. This additional refinement was deemed unnecessary at the low Froude numbers of concern to the ship wake problem of interest and was therefore not implemented. Insufficient nonlinear data is currently available to accurately evaluate the critical Froude number below which $F = 0$ vortex trajectories are sufficiently accurate. The results show however that Froude numbers below Telste's "moderate" value could be simulated with rigid wall vortex paths. In the cases simulated, the initial separation and depth of the pair are 1.0 and 5.0, respectively.

The "low" Froude number condition results are plotted in Fig 9. Data in this figure correspond to $F = \Gamma/(gS^3)^{1/2} = 0.5$ and a nondimensional time sufficient for the vortices to come to a steady translating horizontal speed below the surface. The x axis in Fig 9 is referenced to the vortex position and nondimensionalized by the initial pair separation distance. It can be seen that the ALM gives very good agreement with the nonlinear method. The slight under prediction of the depth of the surface depression is most likely due to the increase in local dynamic pressure in this region caused by the satisfaction of the surface boundary condition on $y = 0$ in the linearized case. The closer proximity of the free surface to the vortex in the nonlinear method results in a larger induced velocity at the surface, causing a lower dynamic pressure and further

33

surface lowering until an equilibrium is achieved. This figure also shows the influence of neglecting the additional terms (basically the $0.5\phi_x^2$ term) in the solution obtained using the CLM. The absence of induced current terms prevents depression of the surface in the region just above the vortex giving an upward hump rather than a dip in the surface above the vortex.

A comparison of surface displacements for the "moderate" Froude number is shown in Fig 10. The data correspond to $F = 2.236$ and $t = 32$. In this case, the ALM gives qualitative agreement in the surface profile but a vertical offset in predicted elevation. This offset is presumably due to the difference in position of the boundary on which the free surface conditions are satisfied as described in the previous paragraph. The offset error at this Froude number is not considered detrimental as long as the Froude number of the simulations remain below this point. This condition is therefore adopted as the bound in simulation conditions in the data presented in this study.

Overall, the comparison is surprisingly good at low to moderate Froude numbers. In the ambient wave simulations, the moderate Froude number described above was not exceeded due to the unknown quality of surface deformation results in this range.

3.2.4 Effects of Vortex Induced Current on Ambient Waves

The maximum induced surface velocity from a single vortex and its oppositely signed image above the surface can be written as $v_i = \Gamma/\pi L$, where L is the depth of the vortex from the surface. The ambient wave group velocity is defined by $v_a = 0.5(g\lambda/2\pi)^{1/2}$ for linearized deep water waves (Newman[11]). The

ratio of these velocities can be represented using the previously defined nondimensional variables in the following way (where L is approximated by $S/2\lambda$):

$$v_i/v_s = 4 \ F/(S/\lambda) \qquad\qquad \text{where } F = \Gamma/(2\pi g\lambda^3)^{1/2}$$

S represents 1/2 the depth of the vortex divided by the ambient wavelength and its use here is a precursor to the geometric conditions of the vortex pair to be studied in detail in the next chapter. The case study of induced current effects involves comparison of identical flow simulation with and without induced current terms in the free surface boundary conditions. Specifically, the $0.5\phi_0^2 +$ $\phi_0\phi_1$ terms are removed from the dynamic boundary condition. The case chosen for this comparison contains parameter values of $F = 0.2$ and $S/\lambda = 1$ and is described further in the Froude Number Variation section later. Figures 11 and 12 show the corresponding results in a format deserving some description. The surface profile is plotted in each figure for a series of times corresponding to the period of the undisturbed ambient wave. Each profile is offset the indicated amount to prevent overlapping and facilitate comparison at different times. Horizontal lines are drawn for each profile at the $y \approx 0$ value and their indicated spacing provides the vertical scale for wave amplitude measurement. These figures show the dramatic effect the induced current has on changing the length of the ambient waves in the region above the vortices. Wavelength here is loosely defined as the distance between peaks in the surface elevation. Without the current, the maximum stretched wavelength is approximately $130\pm5\%$ of the original wavelength at $t = 13T$ (T = period of ambient wave). The induced current case, over the same time scale produces wavelengths of $210\pm5\%$ the

35

original wavelength. The shortest waves at $t = 13T$ are $80\pm5\%$ and $50\pm5\%$ of the original wavelength in cases without and with current terms, respectively.

The next step is to identify how the parameters of a certain problem (in this case the vortex pair) influence this induced current, and what form of wave modifications are expected.
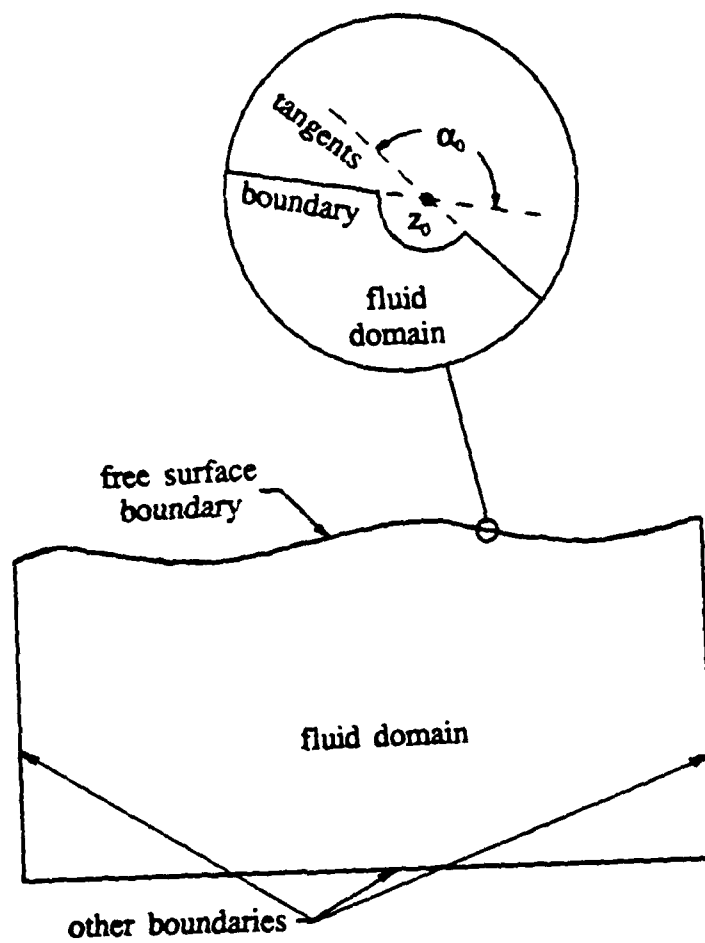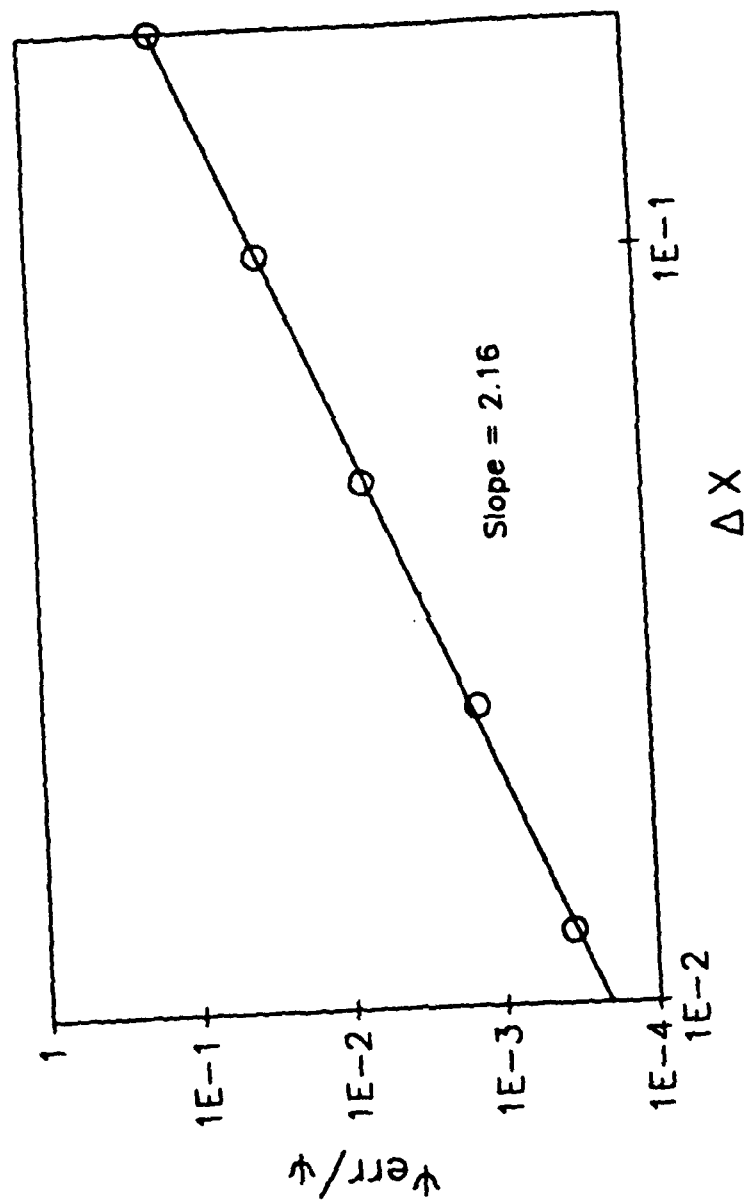
Figure 5 - BIT Domain Description
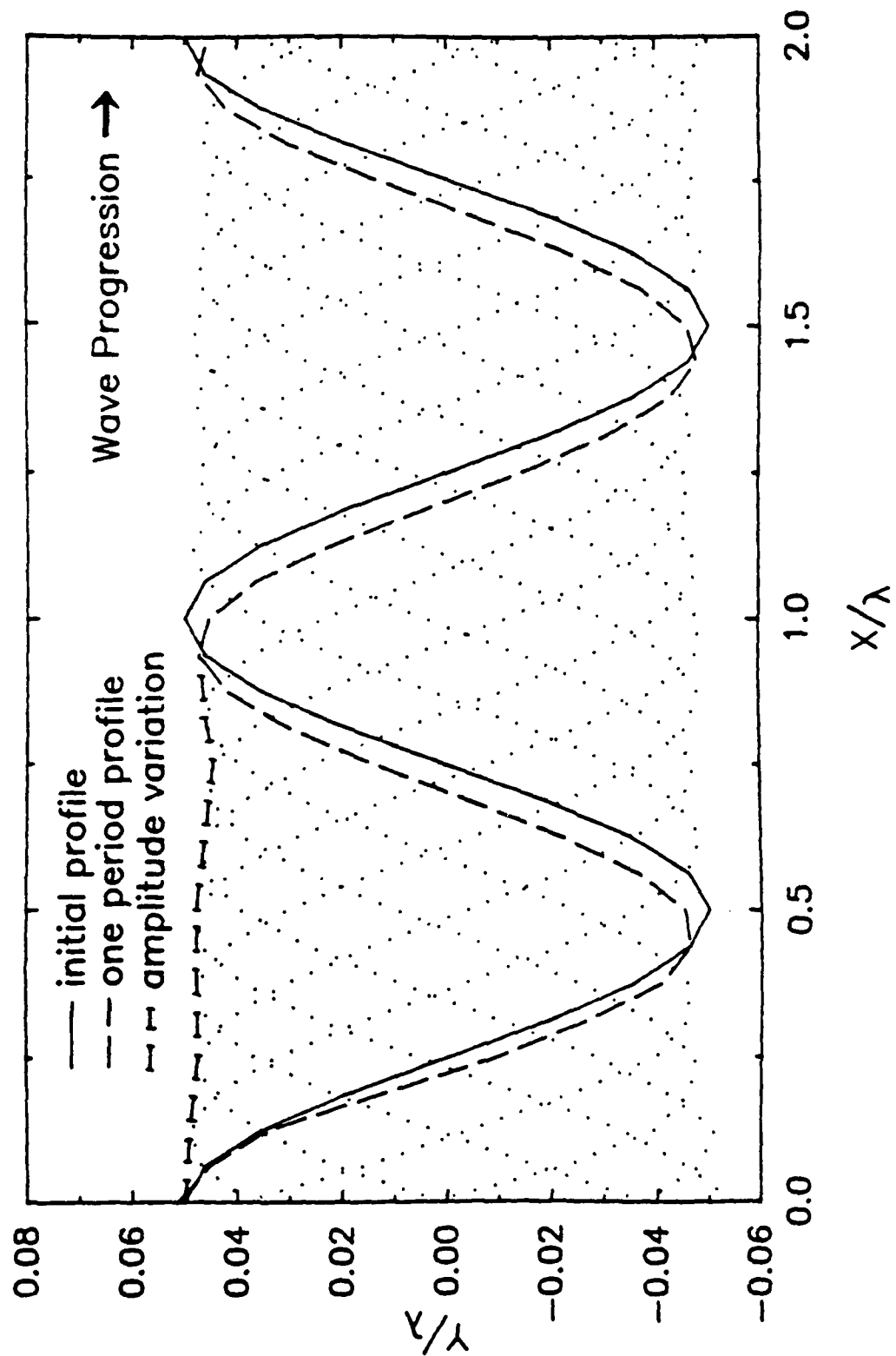
Figure 6 - Cauchy Integration Error
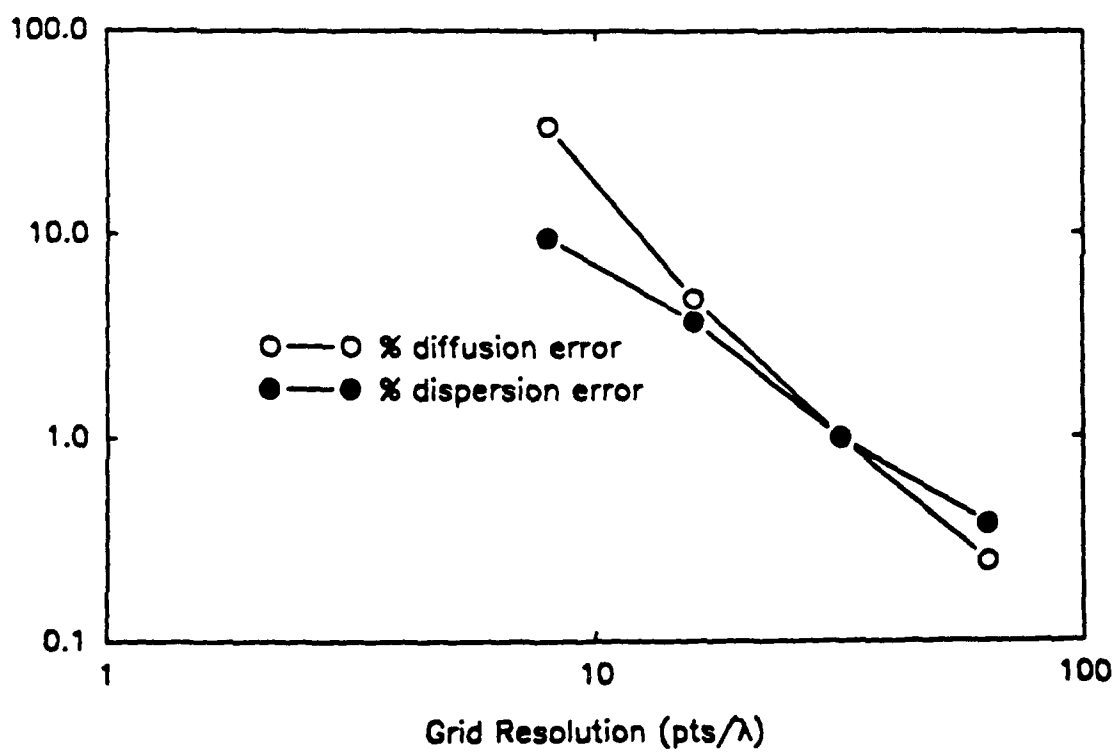
38

Figure 7 - Wave Profile Progression Error

39

Figure 8 - Grid Resolution Effects on Progression Error
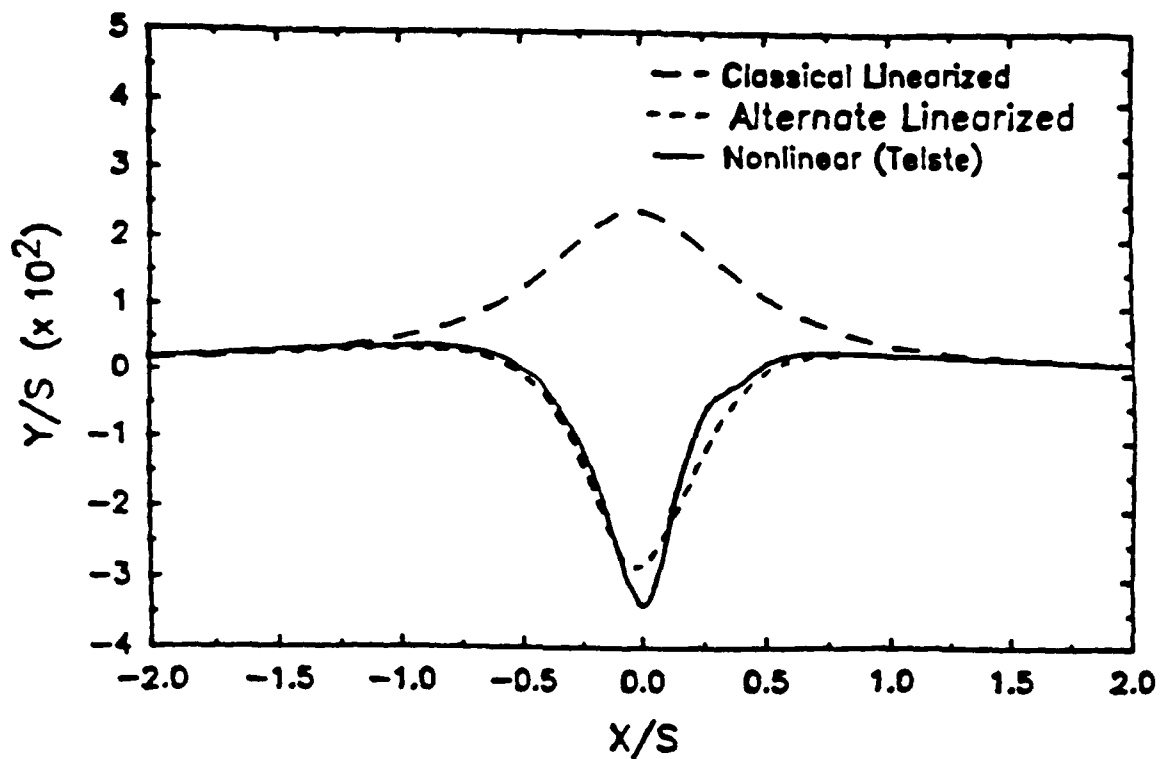
Figure 9 - Low Froude Number: Comparison of Theories
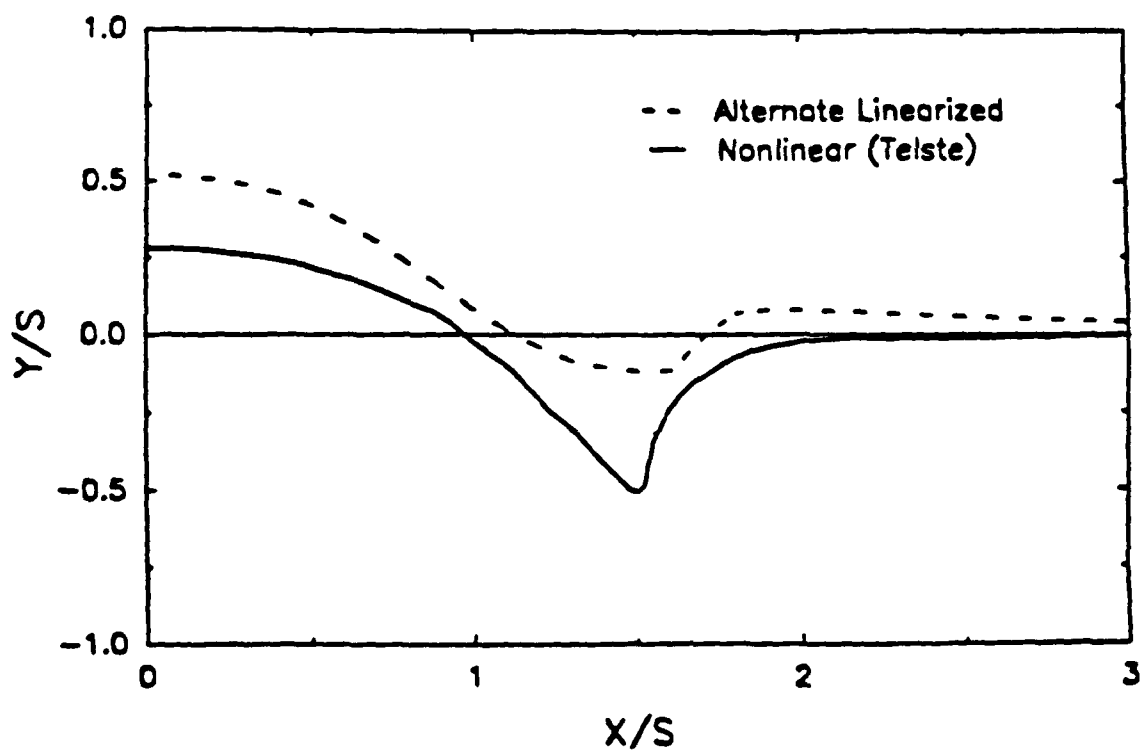
Figure 10 - Moderate Froude Number: Comparison of Theories

41
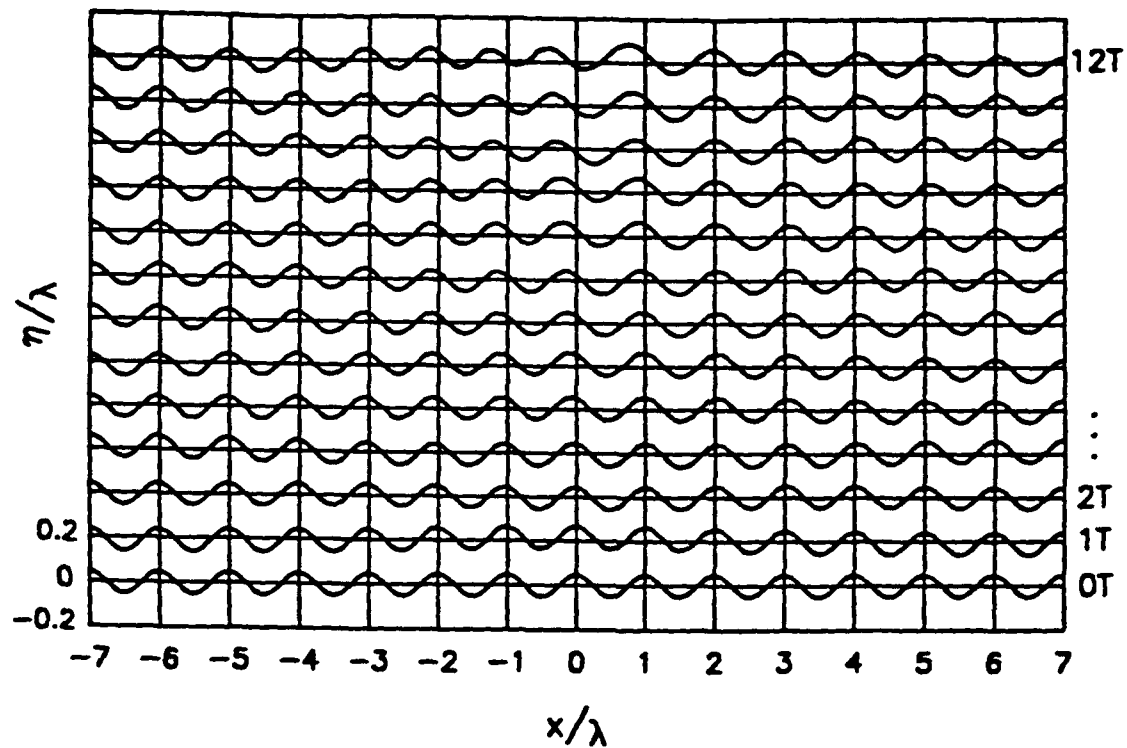
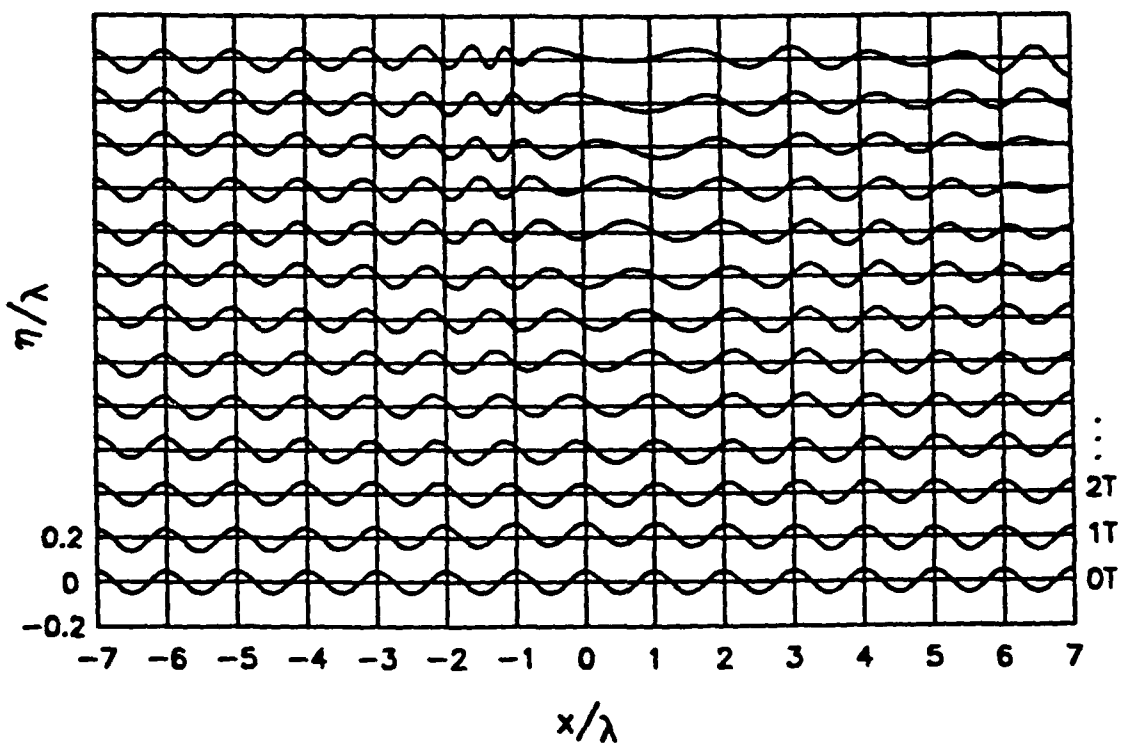Figure 11 - Ambient Wave Modification: Classical Linearization

Figure 12 - Ambient Wave Modification: Alternate Linearization

42

CHAPTER 4 - PARAMETRIC STUDY

4.1 NONDIMENSIONAL PARAMETER IDENTIFICATION

The incorporation of ambient waves into the problem results in the addition of a two new length scales, namely the length and amplitude of the wave. The previously derived boundary conditions need coefficient modification to incorporate these additional parameters. Because the wavelength is directly related to the linearized wave group velocity by the following equation: $V_g = 0.5(g\lambda/2\pi)^{1/2}$, the group velocity could be held constant by nondimensionalizing variables based on the ambient wavelength scale. This resulted in the following nondimensionalization scheme:

$$x = x'/\lambda \quad y = y'/\lambda \quad \eta = \eta'/\lambda \quad \phi = \phi'/\Gamma \quad t = t'\lambda^2/\Gamma$$

$$F = \Gamma/(gS^3)^{1/2} \quad P = A/\lambda \quad Q = S/\lambda \quad R = S/D$$

where ' indicates dimensional quantity, and

   Γ = vortex circulation

   S = inital vortex pair separation

   D = initial vortex pair depth

   λ = ambient wavelength

   A = ambient wave amplitude

Substituting these relations into the previously defined ALM boundary conditions gives the following results:

<u>kinematic boundary condition:</u> $\eta_t = \phi_y + \eta\phi_{0_{yy}} - \phi_0\eta_x$

<u>dynamic boundary condition:</u> $\phi_t = -\phi_{0_x}^2/2 - \phi_0\phi_{1_x} - \eta/(F^2 Q^3)$

The corresponding deepwater wave potential using the above nondimensional parameters takes the form:

$$\phi_w = P/(F\,Q^{3/2}\,(2\pi)^{1/2})\,\exp^{2\pi y}\,\sin\,[2\pi x - (2\pi)^{1/2}t/(F\,Q^{3/2})]$$

The vortex potential is also nondimensionalized and given below in complex form:

$$\beta_0 = \phi_0 + i\psi_0 = 1/i\,\ln\,[(z-z_1)/(z-z_2)] - 1/i\,\ln\,[(z-z^*_1)/(z-z^*_2)]$$

where the "*" character represents complex conjugate. This collection of equations show the three parameters, F, P and Q as intrinsic coefficients. F is the familiar Froude number for vortex pairs with a still free surface. P, or A/λ, represents the steepness ratio of the ambient waves. Q, or S/λ, is a scaling parameter between the vortex spacing and the ambient wavelength. R, or S/D, will be shown later to represent the initial position of the vortices on their predefined paths. Since S/D and S/λ are both related to the initial geometric conditions of the vortex pair their influence will be grouped together. Before proceeding further, these geometric parameters and the associated vortex paths prescribed will be described.

As a consequence of the linearization as discussed in the previous chapter, the vortex trajectories follow the paths of F = 0 solutions. The paths prescribed for this rigid free surface condition were first described by Lamb[7] as

$$a^2(x^2+y^2) = 4x^2y^2 \qquad \text{where "a" is an arbitrary constant.} \qquad (8)$$

Paths corresponding to this equation with different values of "a²" are plotted in Fig 13. It should be noted that the vortex strength is excluded from this path definition. The only role the vortex strength plays is in determining the speed at which the vortices move along thier paths. Since the vortices must follow one of

44

the paths shown, their positions can be determined by knowing their start point, their strength, and the elapsed time. This figure also shows that the final depth of the vortices is equal to half the initial separation distance if the initial start point was relatively deep (small S/D). Cases of vortex depth less than half of the ambient wavelength were avoided due to the inherent errors introduced in vortex paths caused by wave induced velocities at these shallow depths.

4.2 OUTPUT FORMAT DESCRIPTION

The output of the transient simulation is the free surface profile as a function of the nondimensional time variable. The quantity of output generated is, however, somewhat cumbersome in its raw form due to the large number of free surface grid points and time steps. Three dimensional surfaces composed of the 2-dimensional free surface profiles stacked in time can be used for qualitative observation of the data, but a more direct 2-dimensional presentation of segments of the data will be used as the primary presentation form. These 2-dimensional plots will show the surface profile at intervals of time corresponding to the period of the ambient wave. Each surface profile is offset vertically to differentiate it from the others but maintains the same scale for comparison. The sampling of the output at periodic intervals results in very little qualitative loss in comprehension of the flow due to the continuous nature of the surface evolution as verified in the 3-dimensional surface representations. This can be seen in Figs 14 and 15 representing a typical data set. Figure 14 shows the results of partial wave reflection on the right side. These ambient wave reflections form a pattern

45

similar to standing waves. Figure 14 also shows the shortening and elongation process as a bending of wave crest lines in time.

4.3 FROUDE NUMBER VARIATION

The Froude number for this problem can be defined in several ways depending on one's choice of length scale. The traditional length scale chosen in studies without ambient waves is the initial vortex separation distance. The resulting form of the Froude number is $F = \Gamma/(gS^3)^{1/2}$. The examination of Froude number influences will consist of flow simulations with the vortices started at a relatively deep position (S/D $=$ 1/3). This value of S/D was chosen to minimize surface disturbances associated with the transients of the vortices' impulsive start. The ambient wave modifications would therefore $\vdash$ associated predominately with the velocity field generated by the slowly moving vortices rather than the initial condition wave motion generated by the vortices. S/D = 1/3 also corresponds well with the experimental studies of Willmarth et.al.[22] described earlier. S/λ was set equal to 1 as an example ratio. This value of S/λ allows one to consider the Froude number to be based on the length scale of the ambient waves $F_\lambda = F Q^{3/2} = \Gamma/(g\lambda^3)^{1/2}$ with no change in its value. The resulting surface profiles for F ranging between 0.1 and 0.6 are shown in Figs 16 to 20. Since the time scale of modification is much slower at F = 0.1, the profiles shown in Fig 16 coincide with 2T intervals rather than the 1T intervals used in Figs 17 to 20. The corresponding vortex paths are shown for comparison in Fig 21. Note in Fig 21 that the vortex paths of each condition have been offset slightly in the x direction to lessen marker overlap. In actuality, all of the paths

are the same, only the sample points along the path differ. The surface modification in these profiles involves a stretching of waves in the center region above the vortices at later times. The ambient waves also appear to be shortened somewhat on the left or "windward" side due to the adverse directions of v_i and v_t. The wave shortening on the right or "leeward" side is much less pronounced since v_i and v_t are in the same direction.

The most obvious effect of varying the F in these cases is the change in time scale for the surface disturbance to develop. The occurrence of ambient wave modification at earlier times at higher F is due primarily to the increase in relative speed of the vortex pair moving towards the surface. To minimize this attribute, surface wave profiles can be compared between different F cases when the vortex pair are at common positions. Two common positions are labeled "A" and "B" in Fig 21. The corresponding profiles from each F are collected and shown in expanded vertical scale in Figs 22 and 23. Case "A" corresponds to a moderately deep vortex pair. Only the higher F cases corresponding to relatively stronger vortices have an influence at this depth, verifying the notion that stronger vortices will influence the surface from greater depths.

A more subtle and interesting difference is observed as the vortex pair draws near the surface at position "B". Here one notices the lengthening of residual ambient waves in the central region above the vortices. This increase in residual wave length is presumably caused by the higher tangential velocity gradients at the surface in cases where F is increased. The width of the disturbed region above the vortex pair does not depend heavily on the value of F_i. Figure 24 shows the vortex induced current for condition B without waves.

47

For threshold values of v_i/v_s above 0.25, the trend in width of effected region increases at least linearly with F_1. The left side position of wave compression in Fig 23 suggests that the real growth of the effected region is less than linear. This discrepancy is most likely due to the time lag in free surface response which increases as the vortex speed is increased.

An additional note on the variation of F is the transition occurring around values of 0.5 of the surface disturbance directly above the vortex pair. At values above 0.5, the creation of a center "hump" appears similar to center humps calculated by Telste[20] at higher Froude numbers without ambient waves. It should be noted that in this case the vortices have not deviated from their rigid wall paths. This indicates a transition Froude number value of 0.5 above which the vortex pair begins dominating the surface profile.

4.4 INITIAL GEOMETRIC CONDITIONS

The initial position of the vortex pair is equally important to its strength in defining the form of ambient wave modification. As noted previously, the ratio of induced surface velocity to ambient wave group velocity is highly dependant on the depth of the vortex. Time scales for the vortex pair to approach the surface from large depths is also obviously dependant on the initial depth and separation distance. The paths of the vortices in all of the cases studied were defined by the rigid surface condition as explained in Chapter I. This family of paths described by equation 8 and shown in Fig 13 show that the position of vortex pair can be identified by two parameters. The parameter S/D specifies the

relative position of the vortex on any of the family of paths. The particular path desired may then be specified by designating a value for either S or D.

4.4.1 S/D Variation

The influence of starting at various points on a given path will be examined first. The controlling parameter in this case is S/D, which determines the initial point on the path. Three values of S/D are examined corresponding to deep (S/D = 0.5), turning (S/D = 2), and shallow (S/D = 6). As shown earlier, the direction of motion of the vortex pair is quite different in each of these cases. The value of F_λ used in these cases was set to 0.125, and the common path chosen corresponded to a final submergence depth of the vortices of D_{final} = λ. Figures 25 to 27 show the resulting profiles and Fig 28 shows the corresponding trajectories of the right side vortex.

4.4.2 S/λ Variation

As mentioned in the S/D section above, initial vortex pair location is important in examining the influences on ambient surface waves. In addition to specifying the portion of the path that the pair will be started on, a particular path must be chosen. The parameter S/λ is used as a path selection parameter for its role in scaling the vortex path geometry to the ambient wavelength. Three values of S/λ were simulated with a constant value of S/D = 6. S/λ values were set to 3.0, 4.5, and 6.0. The upper limit on S/λ is caused by the size limitation of the computational domain, and the influence of partial wave reflections on the right hand boundary. F_λ varied between 0.06 and 0.125 to

49

preserve a v_i/v_s at the surface of 0.5. Surface profiles for these simulations are shown in Figs 29 to 31. The corresponding vortex trajectories are given in Fig 32.

4.4.3 Comments

The profiles shown in this study of geometric conditions on the vortex pair indicate the great complexity of the flow described by the equations outlined previously. The detailed description of the flow field and its dependence on these parameters is therefore unpractical at this stage of development. Several very important general characteristics of the ambient wave modification can be described, however, providing greater understanding of the important physical mechanisms governing the interaction.

The first general characteristic found was the dominance of the instantaneous depth of the vortex pair. This is seen primarily in the difference in surface disturbance caused by the vortex pair initialized at different points on the same path (varying S/D). In the case of S/D = 0.5, the surface is modified only by slight shifting in the waves caused by the small vortex induced surface current. This wave alteration is also noticed to be almost symmetric about the line of symmetry for the vortex paths. This indicates little net exchange of energy between the vortices and the waves as they pass through. As the depth is decreased, the vortex induced surface current grows to the value of the group velocity of the ambient waves, and essentially stops the transfer of ambient wave energy from left to right. Two important processes occur which deserve further attention. First, the ambient waves are shortened as they enter the region of

50

influence of the vortex pair by the apposing induced current. The resultant decrease in ambient wavelength is accompanied by a decrease in the absolute group velocity of the waves. The result of this process, is that ambient waves of higher speed may be halted by vortices of smaller magnitude than that predicted from $v_i/v_t = 1$. The determination of either a critical vortex strength or ambient wave length for wave stoppage is frustrated by the influence of time scales associated with the motion of the vortices and their depth. In addition, the absolute identification of the wave blockage condition threshold is not currently feasible.

A second important process discovered in the simulations is the dynamics of waves caught in the central influence region. These surviving center waves may be left over from the initial ambient wave profile in this region in the shorter time scales. These left over waves are found in greater numbers as S/λ is increased, as shown in Figs 29 to 31. The cases shown in these figures show a quick generation of wave blocking action due to the relatively large value of v_i/v_g. Wave energy may also propagate into the center region when the vortex pairs are initialized at low values of S/D. This energy propagation is facilitated by the cancelling influence of the induced tangential velocity from each of the counter rotating submerged vortices at low values of S/D. The evolution of these center waves is particularly complex in cases of moderate S/D. Initial waves in this region are typically stretched by the surface current gradient. The resulting increase in wavelength gives rise to an increase in phase and group velocity. Because the gravity wave dispersion relation specifies that longer waves move at higher velocity, the central region may be evacuated over a shorter time than that

predicted by ambient wave group velocity. Simulation results were not carried far enough in time to show complete smoothing of the central region due to the influence of partial wave reflection from the right side boundary. Larger surface grids and greater computer time will therefore be necessary to validate this hypothesis.

4.5 A/λ VARIATION

The parameter A/λ found in the derivation of the ALM represents the influence of ambient wave steepness on the interaction process with submerged vortices. To examine its influence a case of $A/\lambda = 1/10$ was simulated and compared with the same case at the baseline $A/\lambda = 1/20$. The resulting profiles from these two cases are shown in Fig 33. The conditions for the comparison were $F_\lambda = 0.125$, $S/D = 2$, and $S/\lambda = 2$. No apparent changes in the results other than a constant scale factor are present. Additional analysis (Fig 34) shows the result of multiplication of the $A/\lambda = 1/20$ elevation results by 2 and subtracting the $A/\lambda = 1/10$ results. From this plot one notices the weak coupling of this parameter with the long wavelength character of the waves generated by the initial conditions of the vortex. This is verified by almost identical results between Fig 34 and simulations with $A/\lambda = 0$. It was concluded from this that the wave steepness parameter plays a minor role in shaping the wave modification region, and provides a roughly linear vertical amplification of simulation profiles.

52

4.6 PHASE VARIATION

Before pursuing spectral analysis of the simulation results, the influence of ambient wave phase must be scrutinized. A sample case is simulated with multiple phase ambient waves and the resultant surface profile shown in Fig 35. This figure shows no significant variation in wave modification as the phase is changed. In addition, the spectral analysis described in the next section was applied to each of these cases with no significant variation associated with the ambient wave phase. The influence of ambient wave phase will therefore be considered secondary to the other parameters of the problem and will be neglected in the spectral analysis to follow.

\
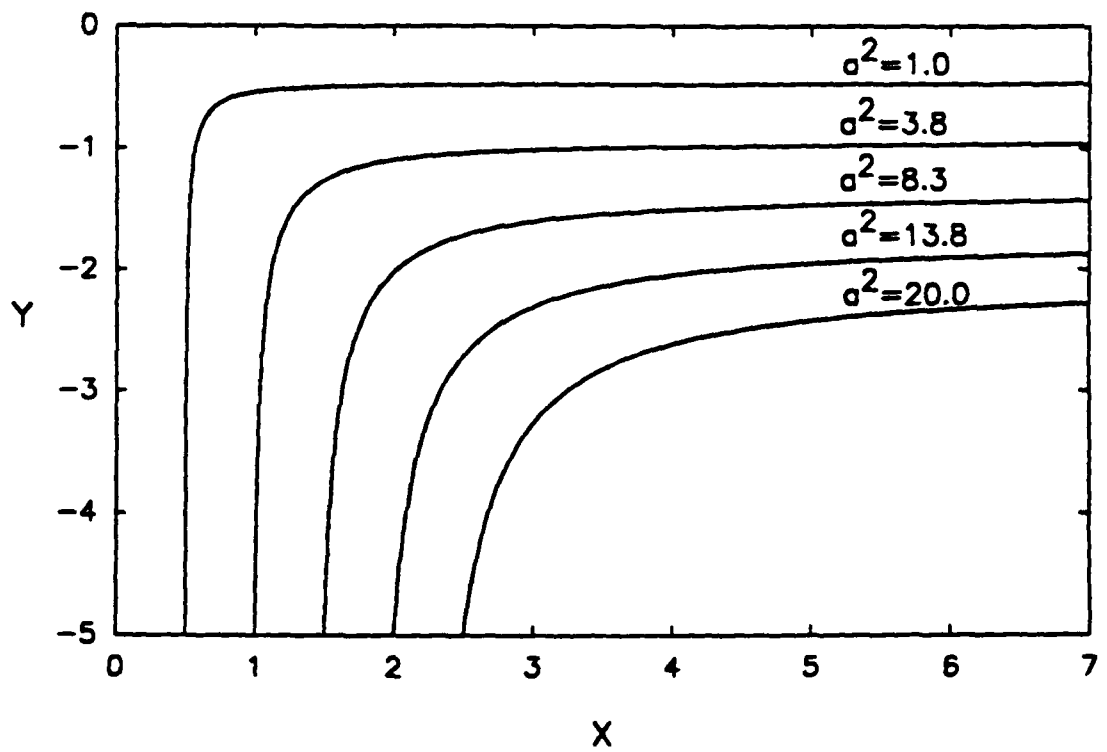
Figure 13 - Low Froude Number Vortex Paths
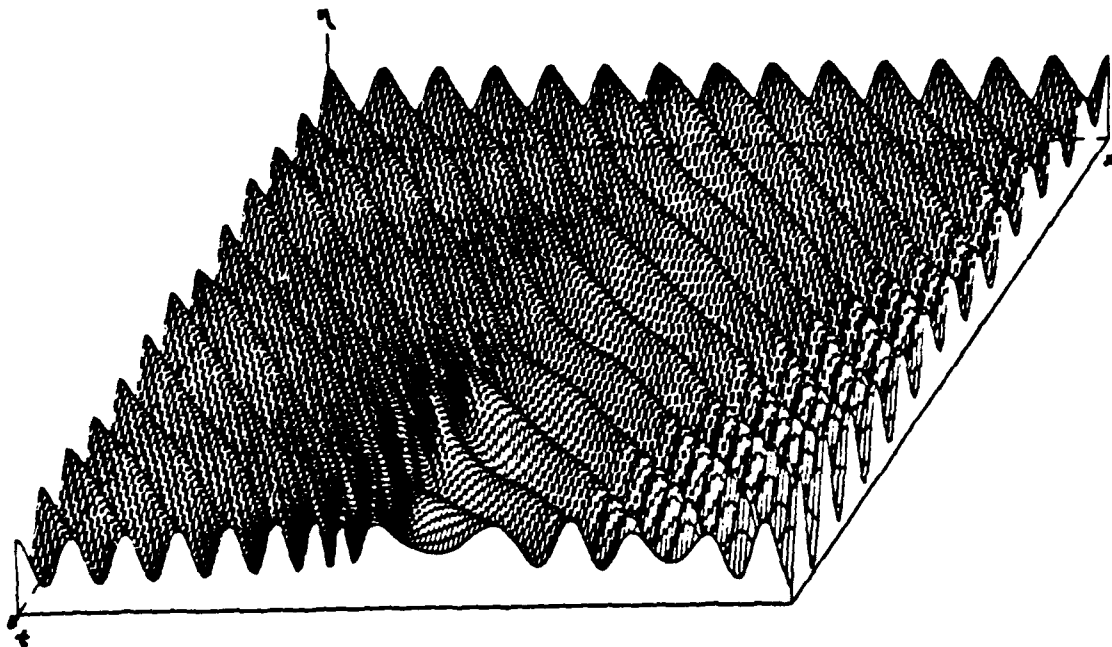
Figure 14 - 3-D Free Surface Representation

η/λ (grid spacing=0.2)

x/λ
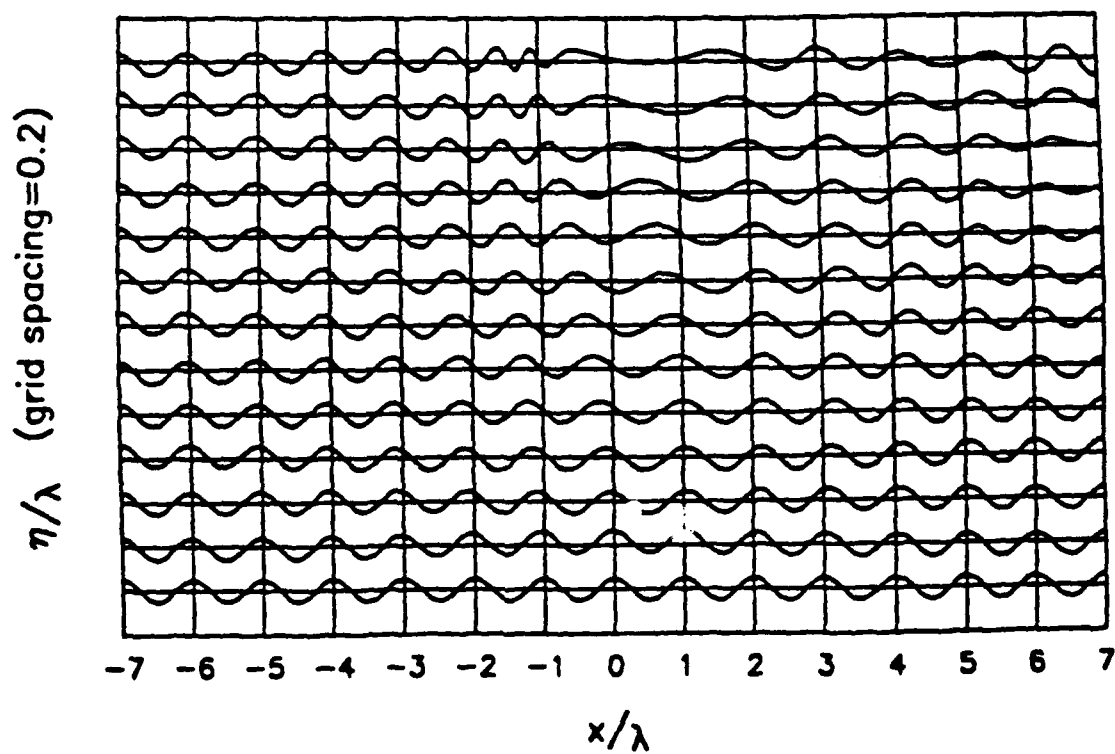
Figure 15 - Discrete Profile Surface Representation
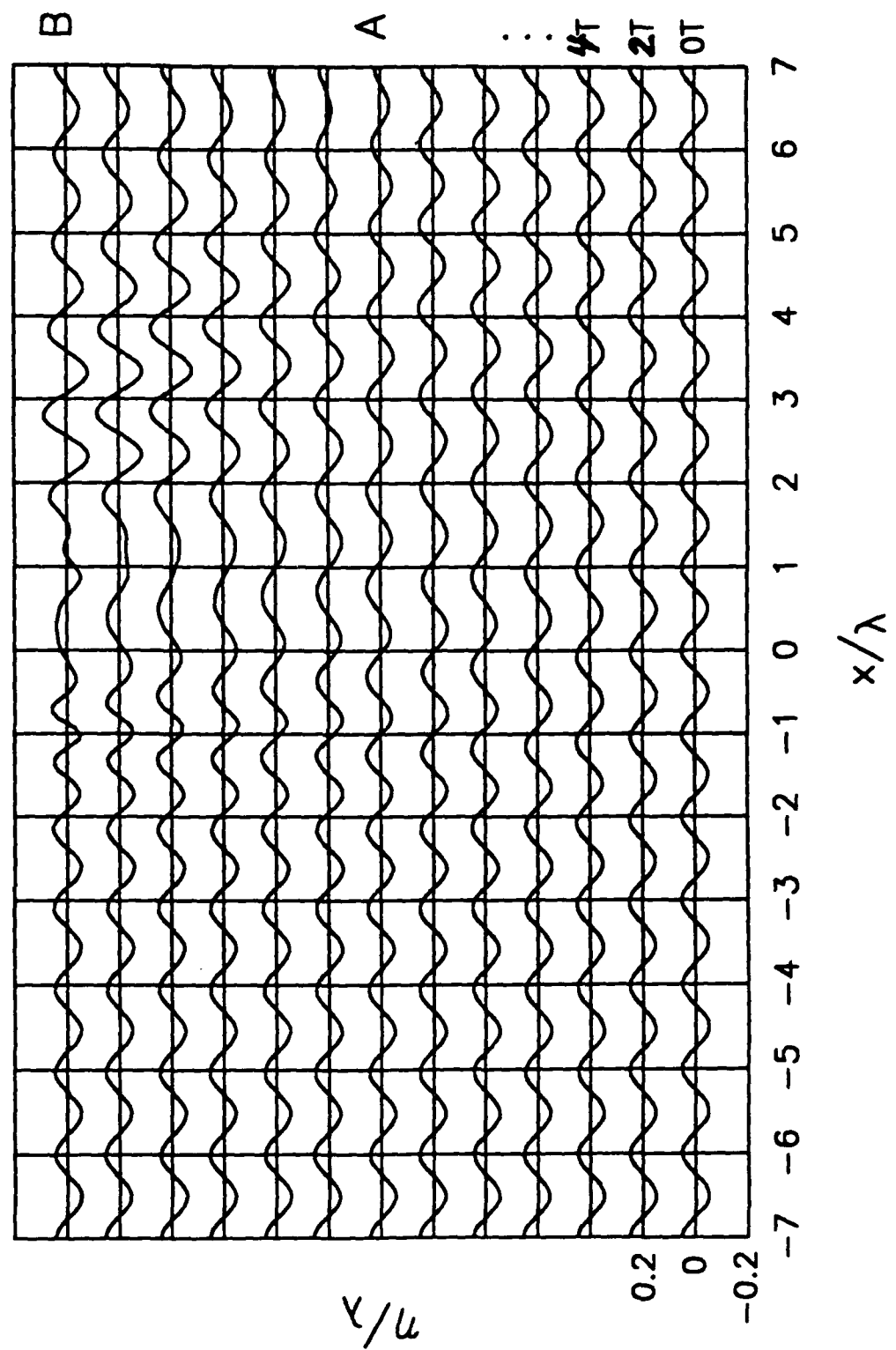
Figure 16 - F Variation: F=0.1, S/D=0.33, S/λ=1

56
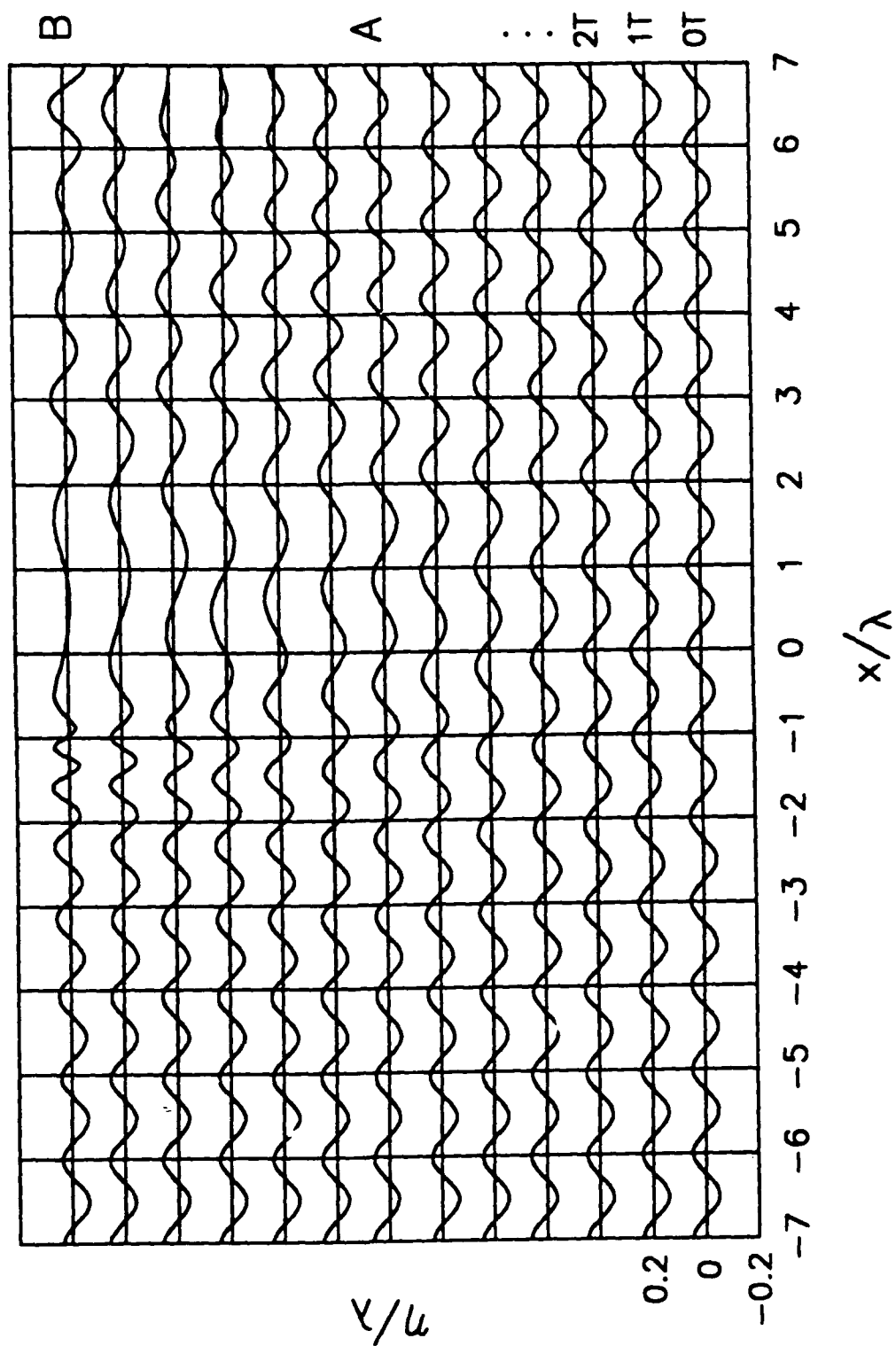
Figure 17 - F Variation: F=0.2, S/D=0.33, S/λ=1

57
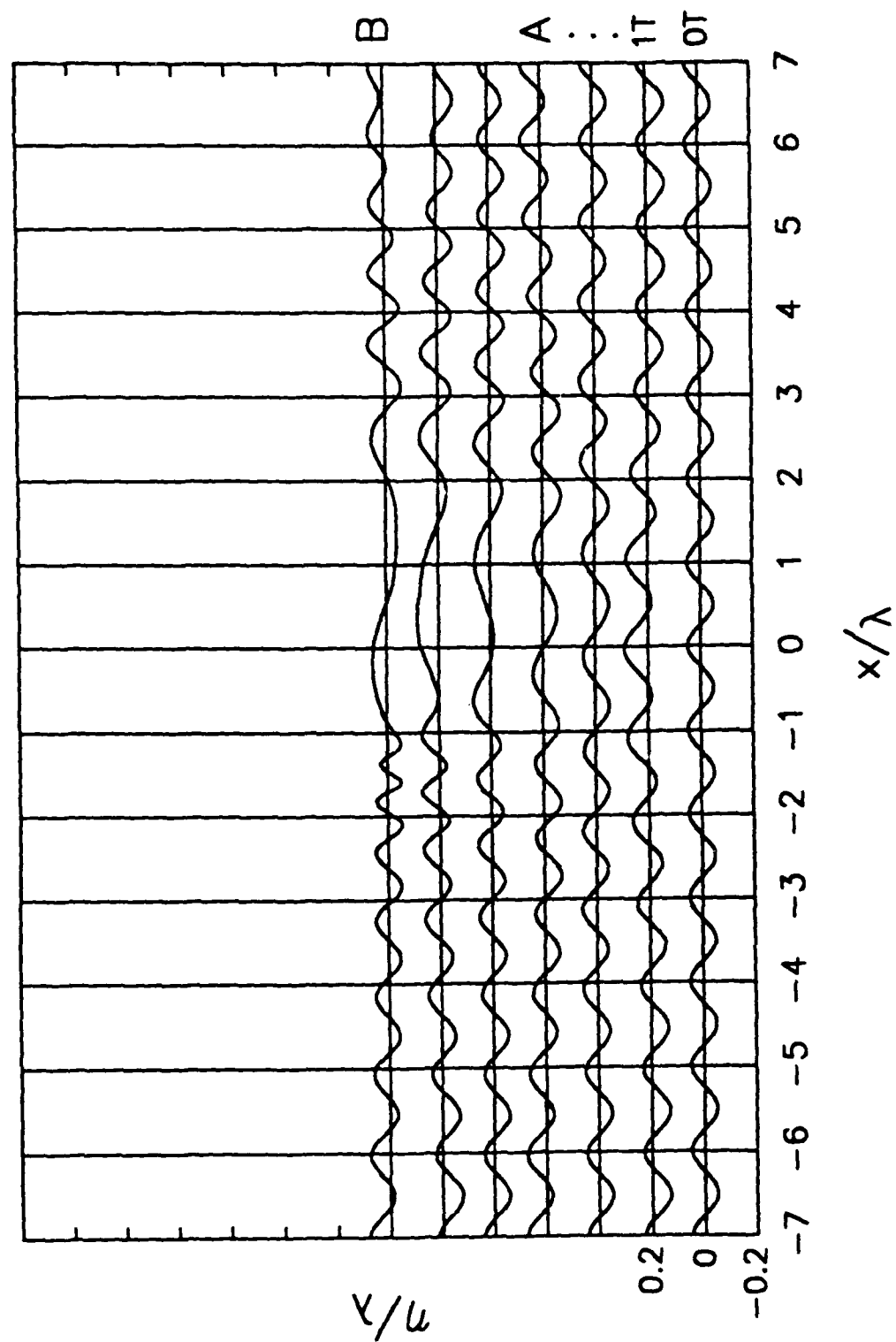
Figure 18 - F Variation: F=0.4, S/D=0.33, S/λ=1

58
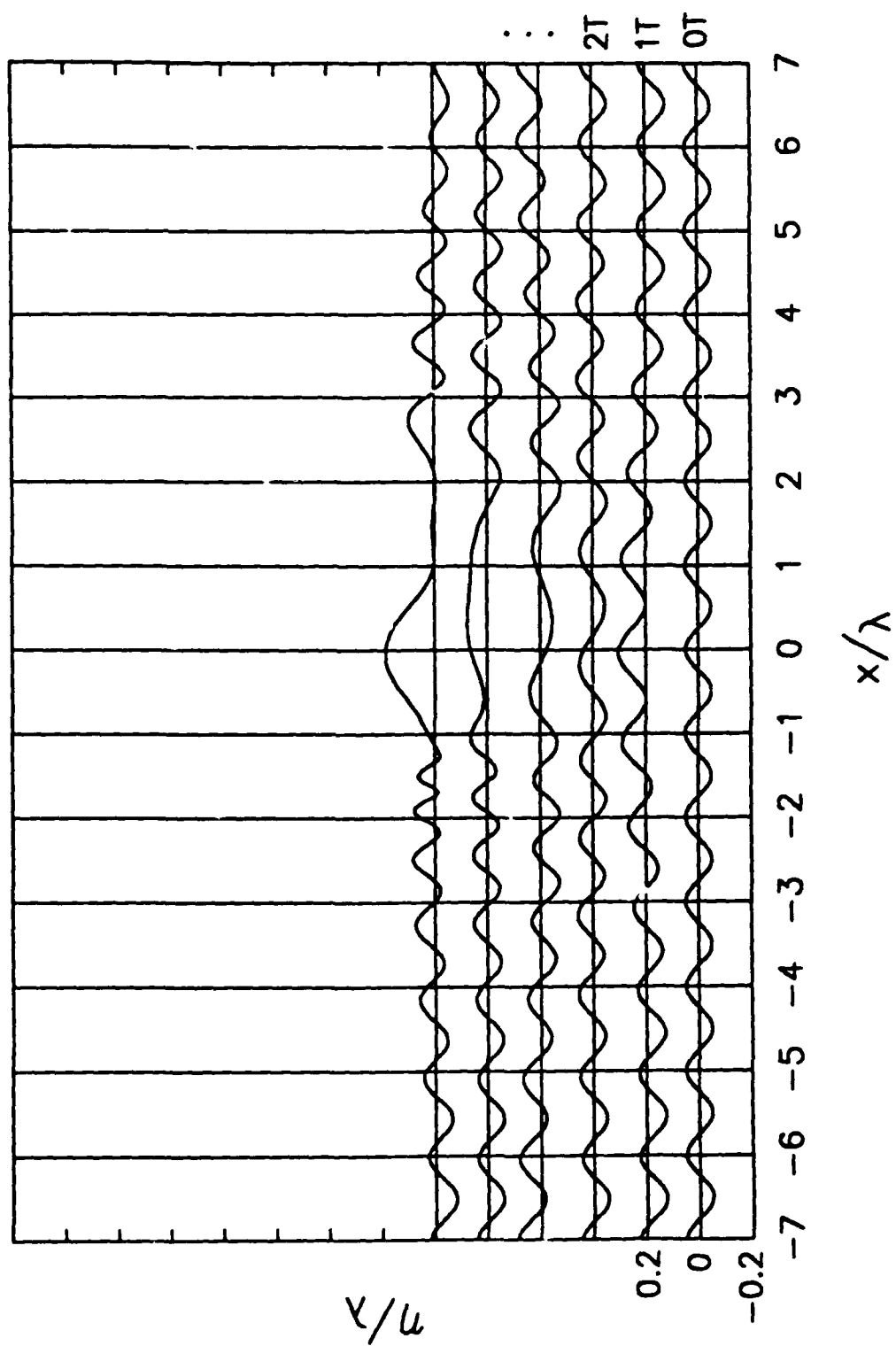
Figure 19 - F Variation: F=0.5, S/D=0.33, S/λ=1

59
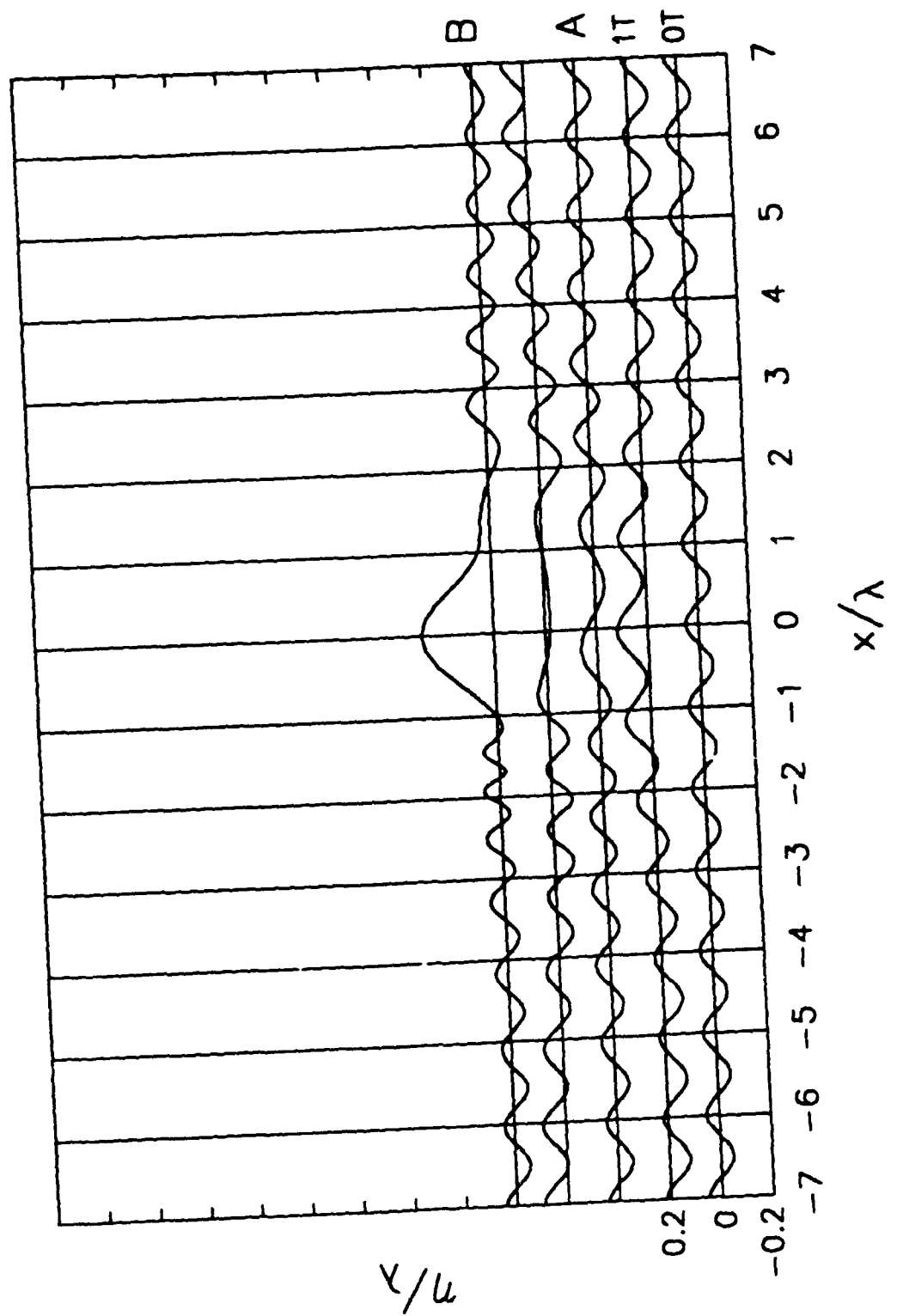
Figure 20 - F Variation: F=0.6, S/D=0.33, S/λ=1

60
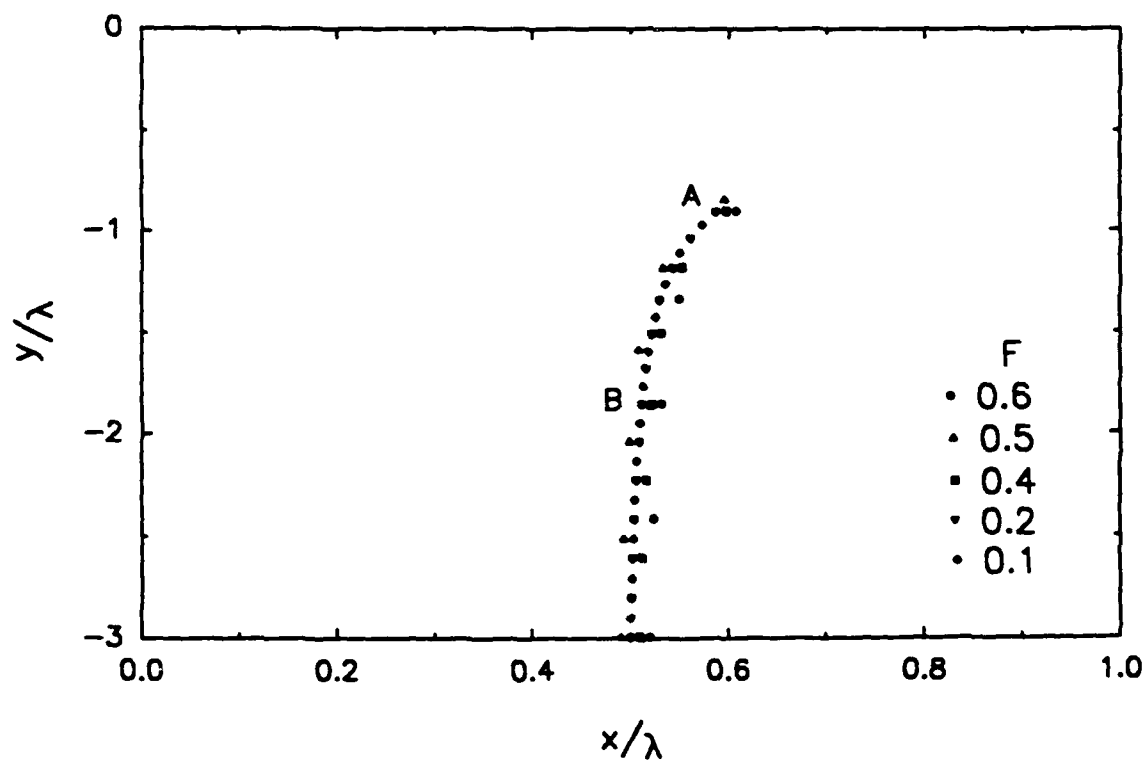
Figure 21 - F Variation: Vortex Paths

61
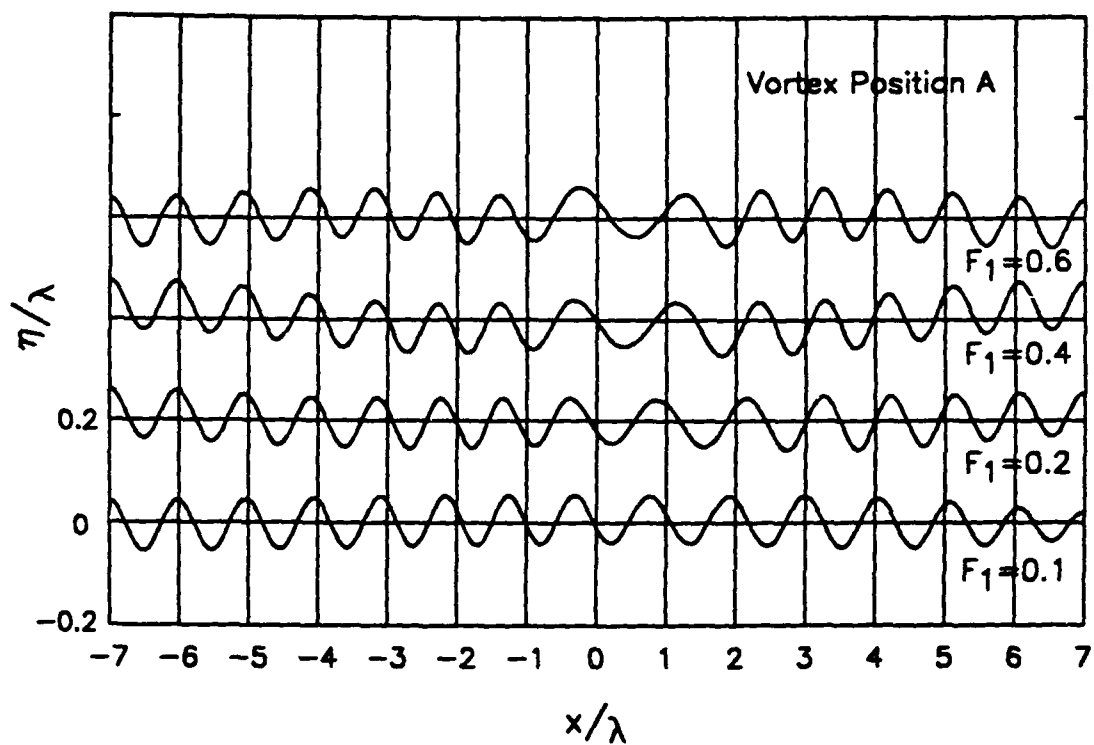
Figure 22 - F Variation: Position "A" Surface Profile Comparison
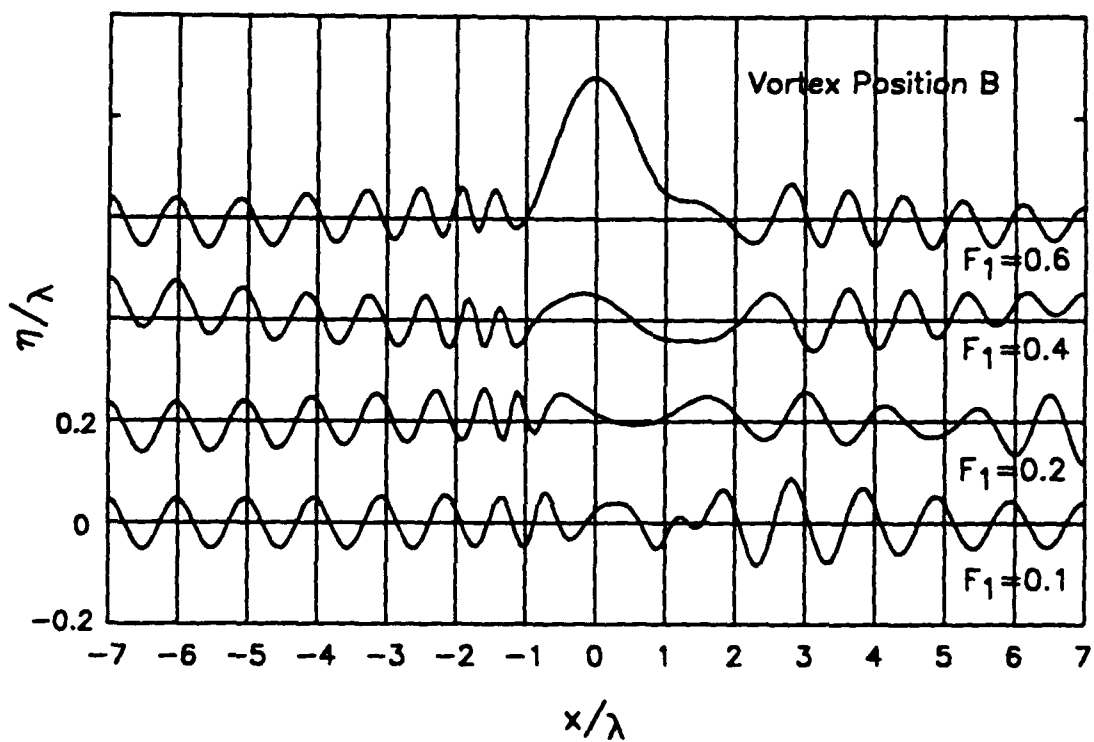
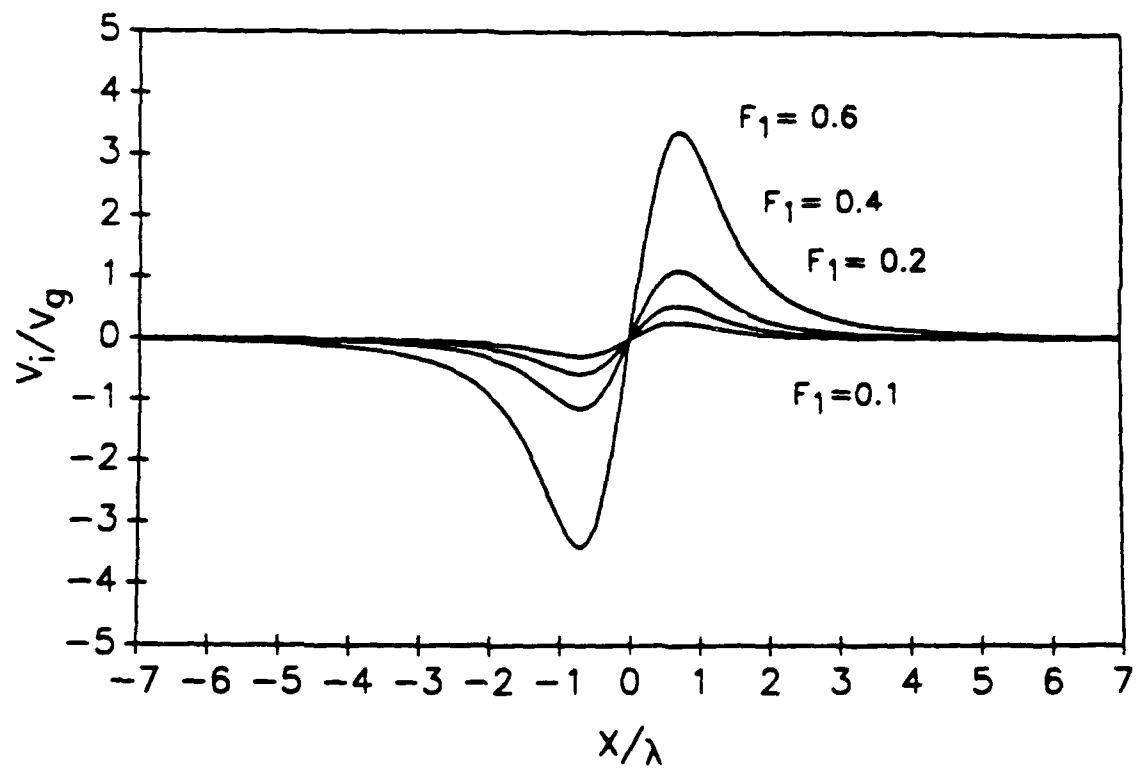Figure 23 - F Variation: Position "B" Surface Profile Comparison

62

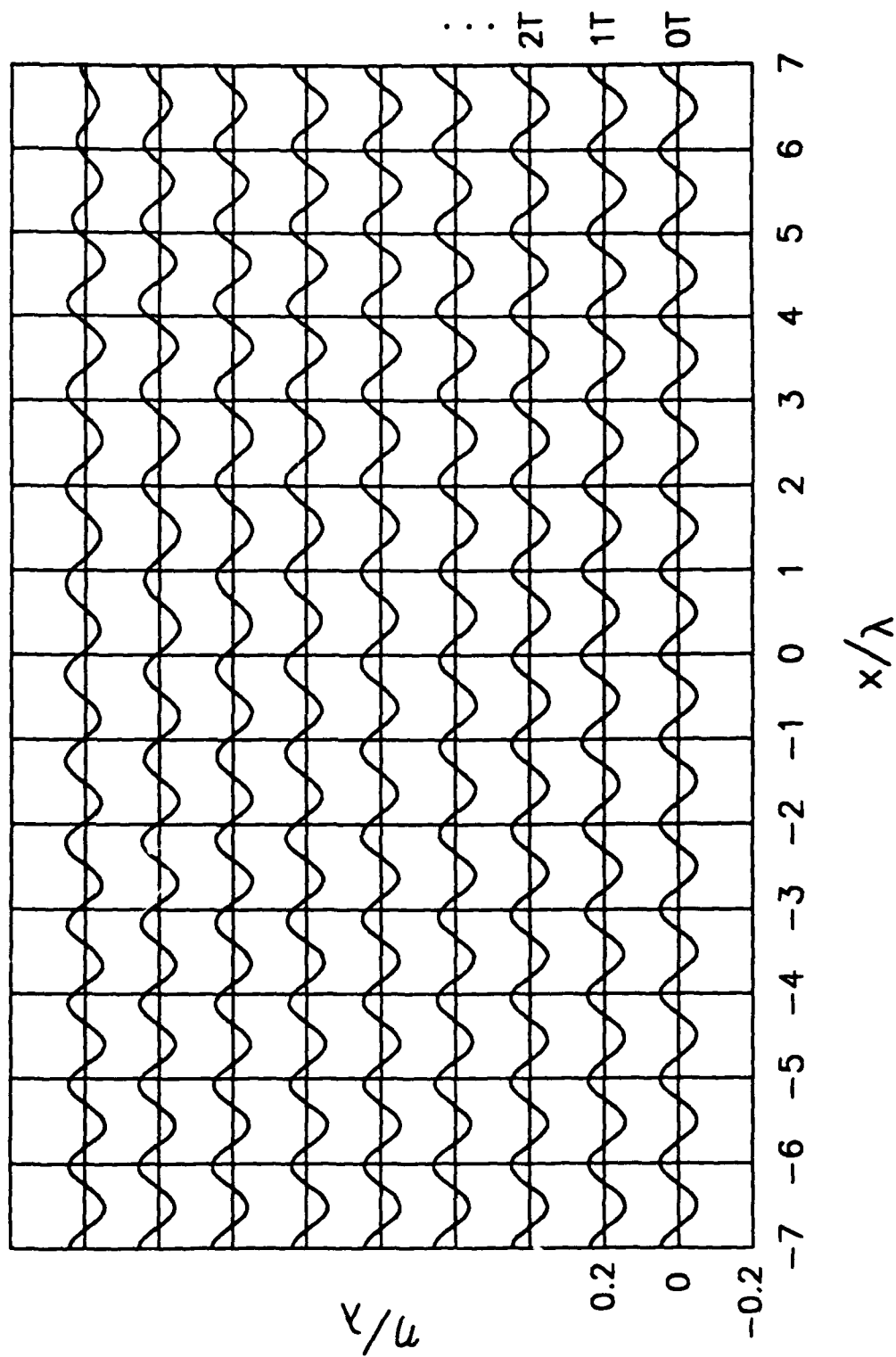Figure 24 - F Variation: Induced Surface Current at Position "B"
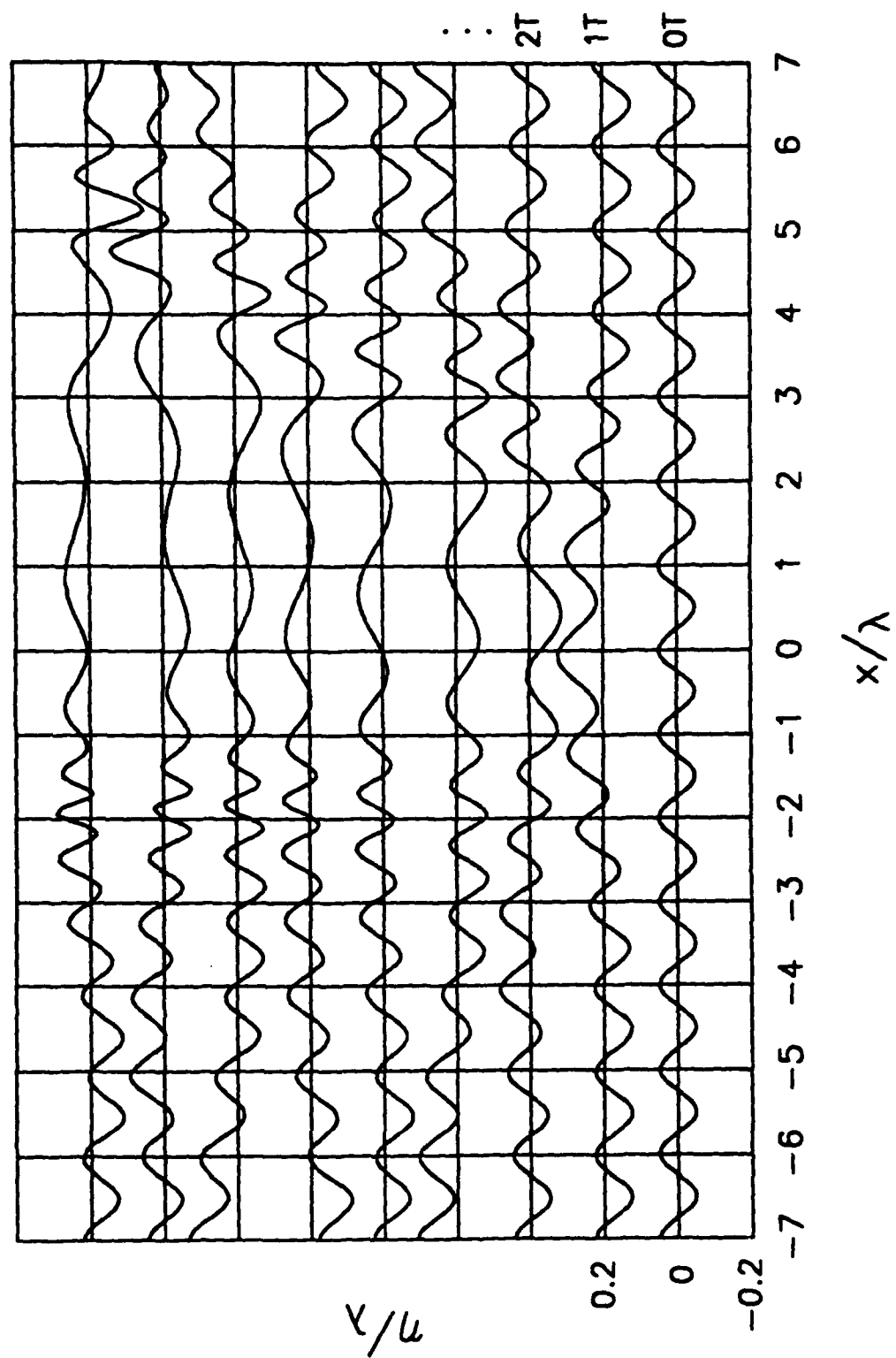
63

Figure 25 - S/D Variation: S/D=0.5, F=0.125, S/λ=2.0
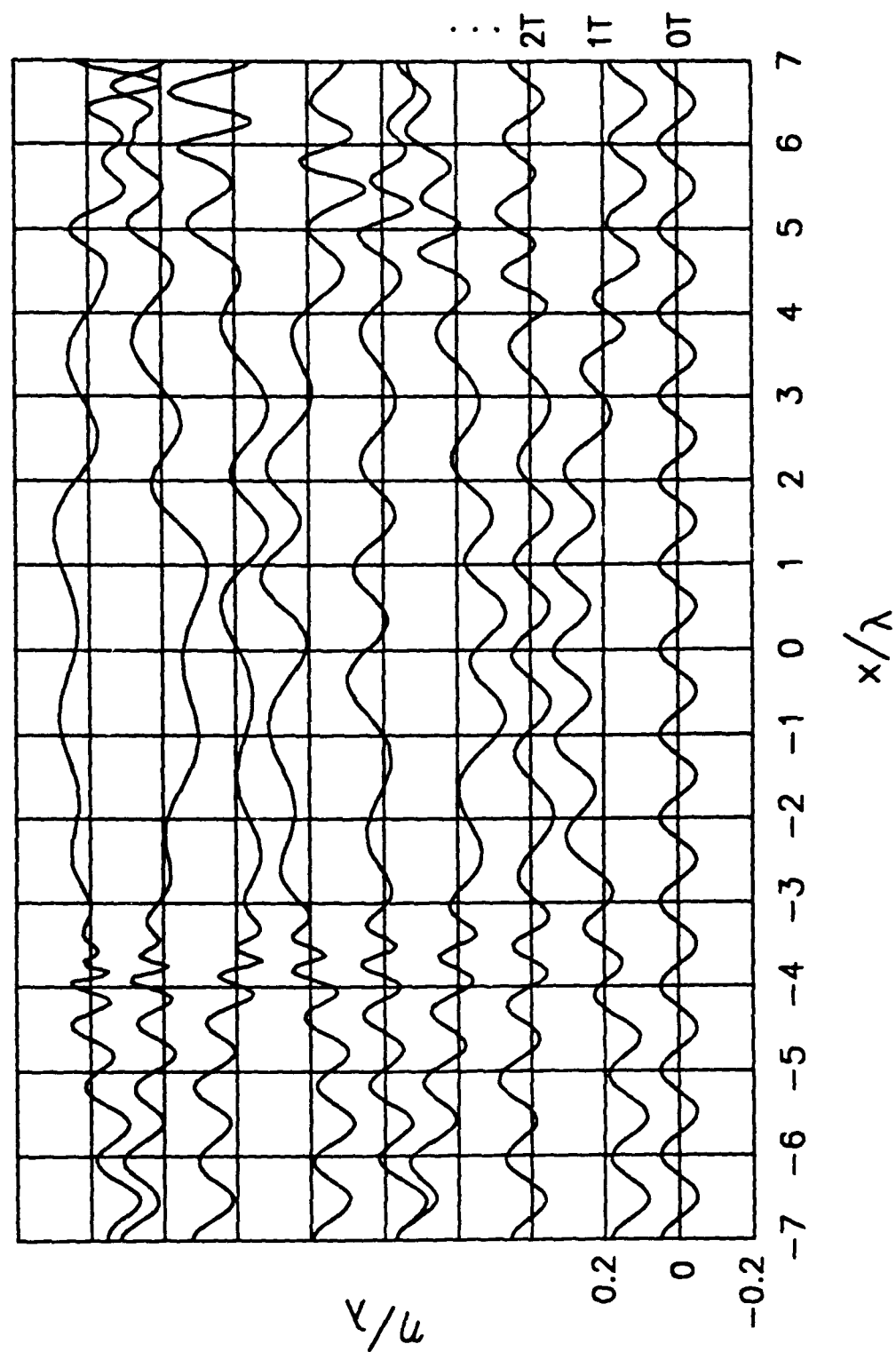
64

Figure 26 - S/D Variation: S/D=2.0, F=0.125, S/λ=2.5

65

Figure 27 - S/D Variation: S/D=6.0, F=0.125, S/λ=6.0

66
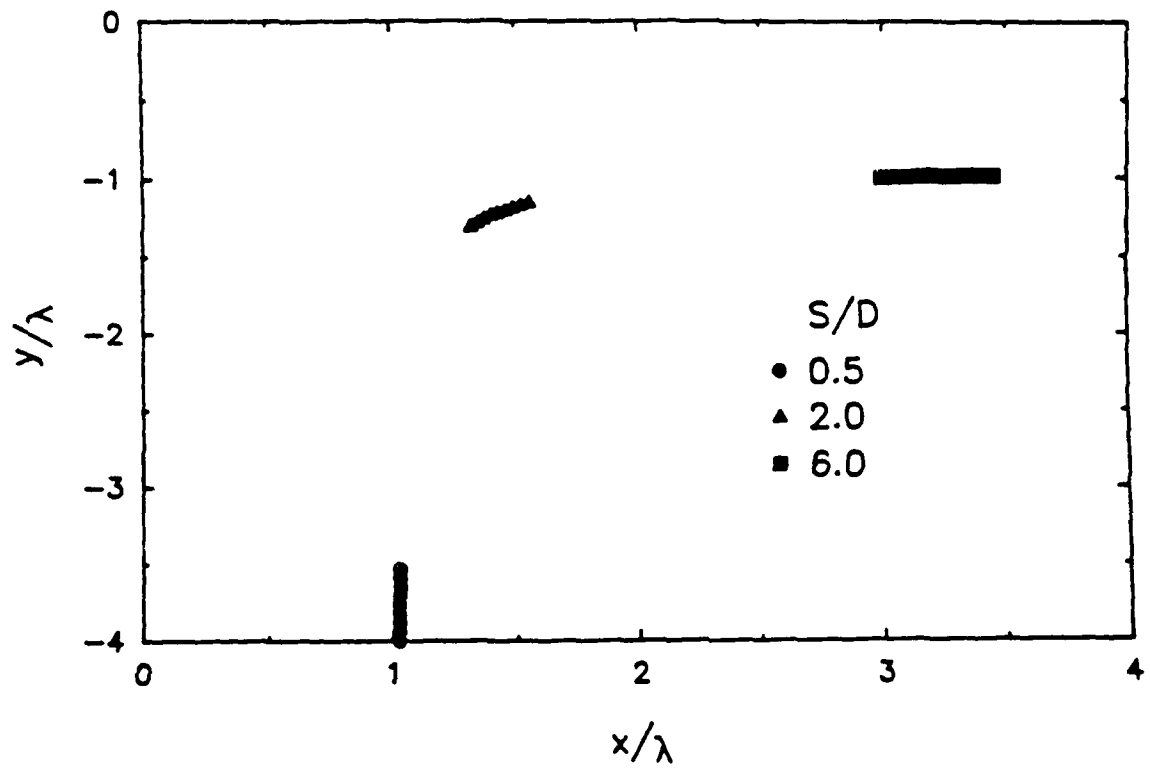
Figure 28 - S/D Variation: Vortex Paths
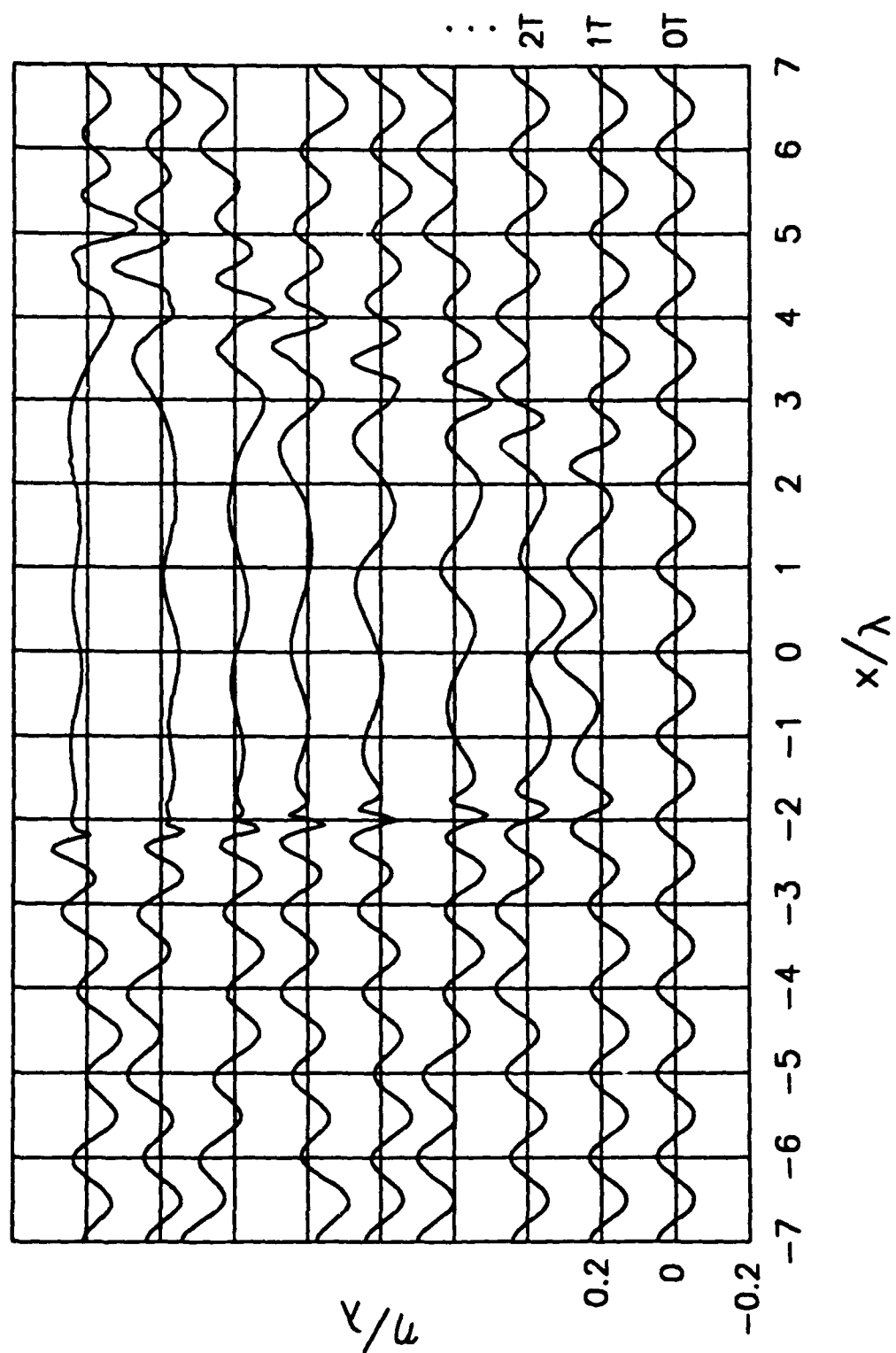
Figure 29 - S/λ Variation: S/λ=3.0, F=0.06, S/D=6.0

68
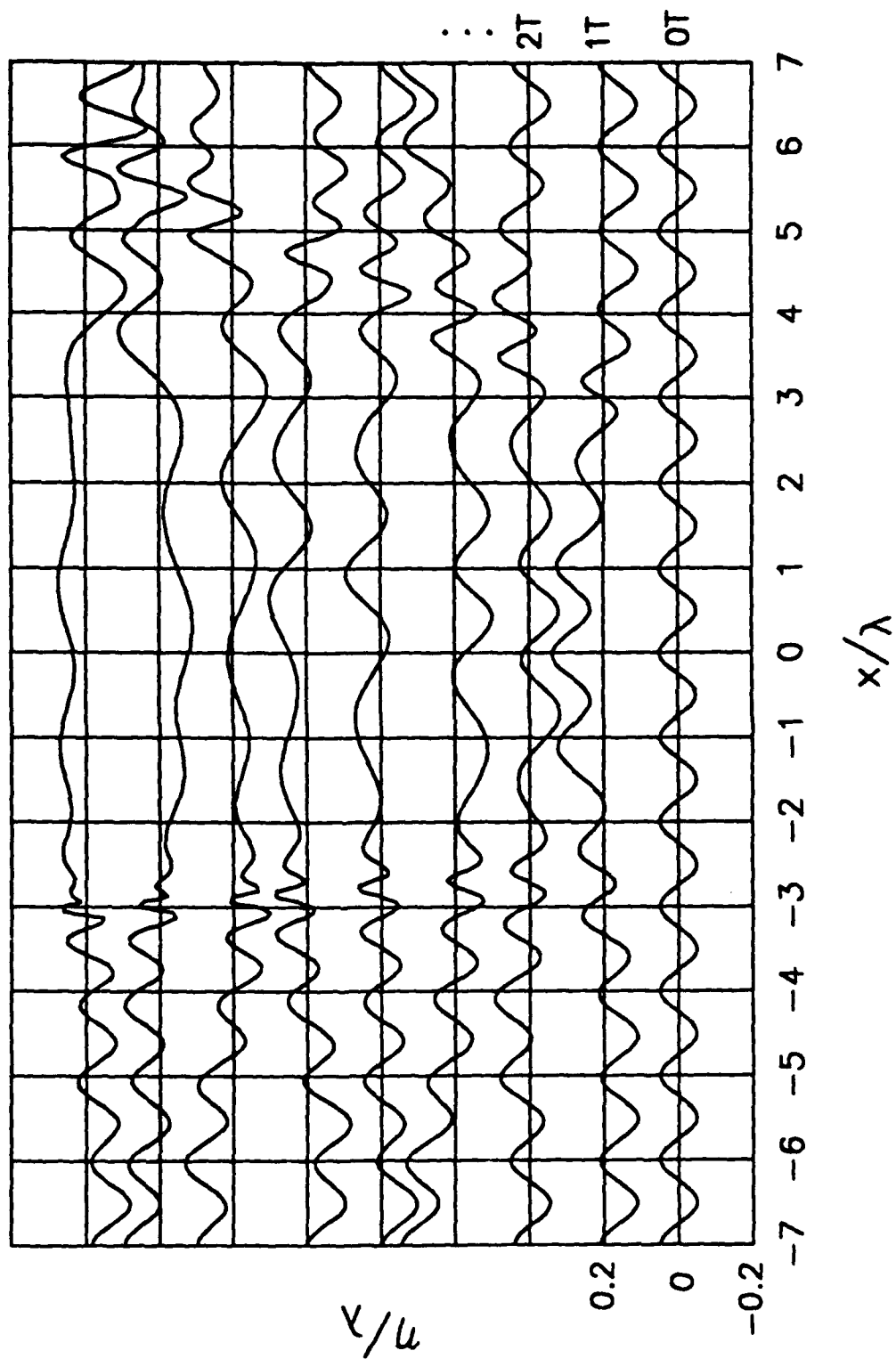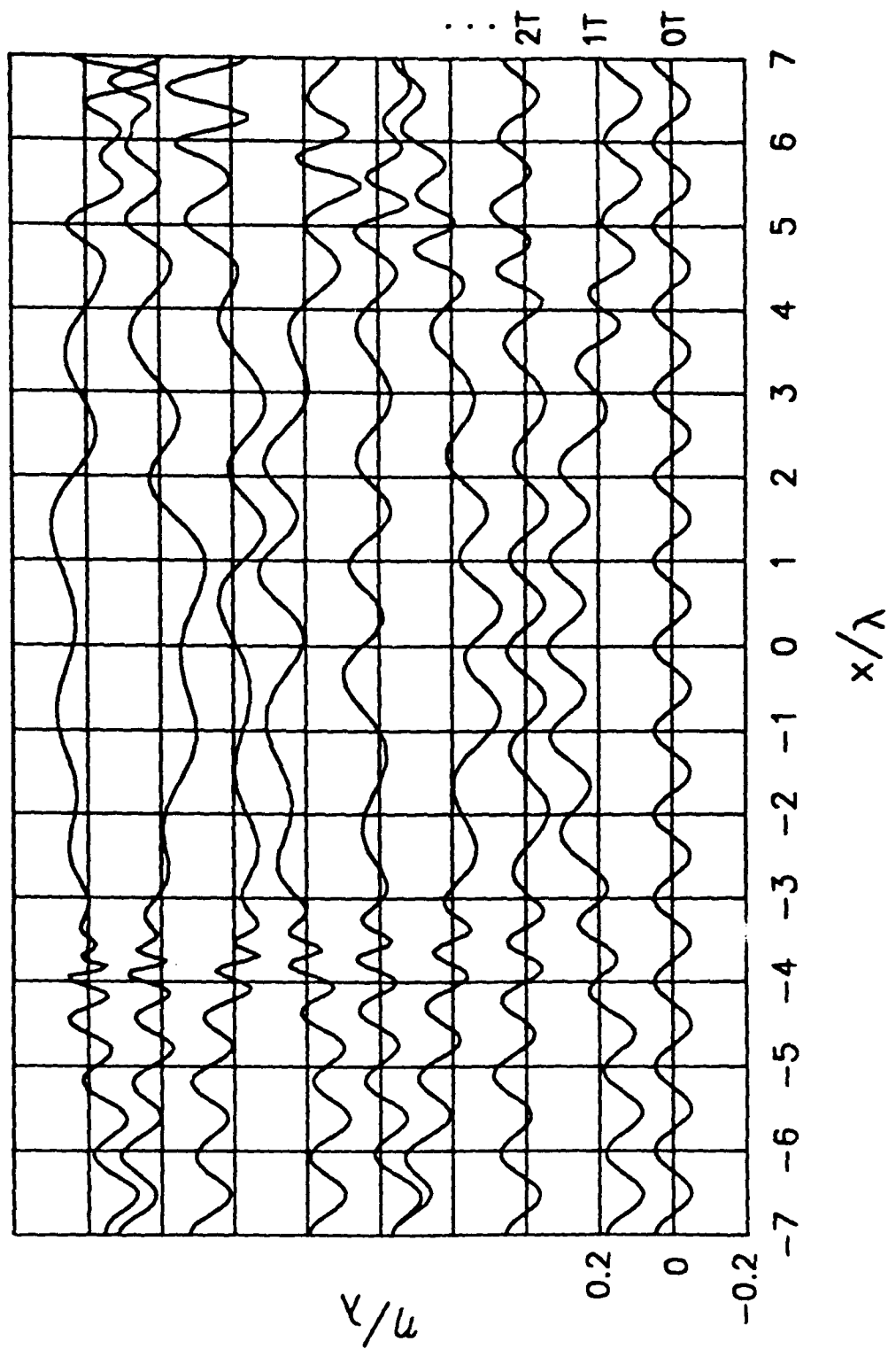
Figure 30 - S/λ Variation: S/λ=4.5, F=0.09, S/D=6.0

69

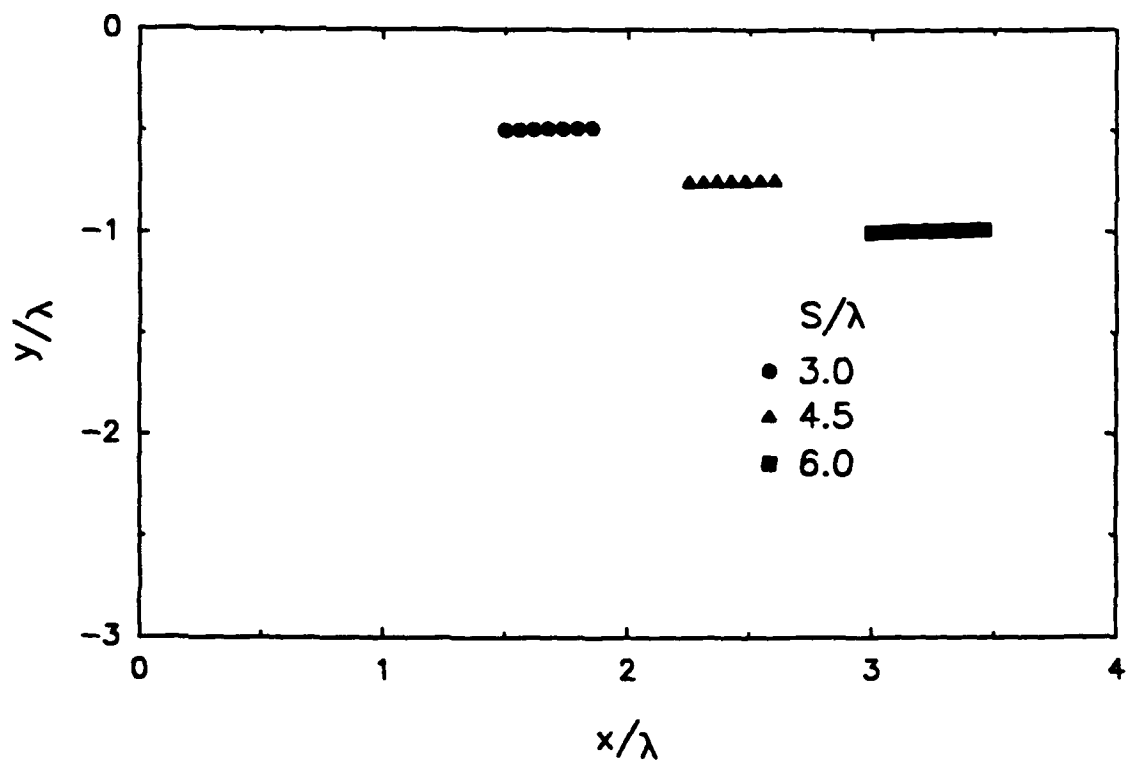Figure 31 - S/λ Variation: S/λ=6.0, F=0.125, S/D=6.0

70

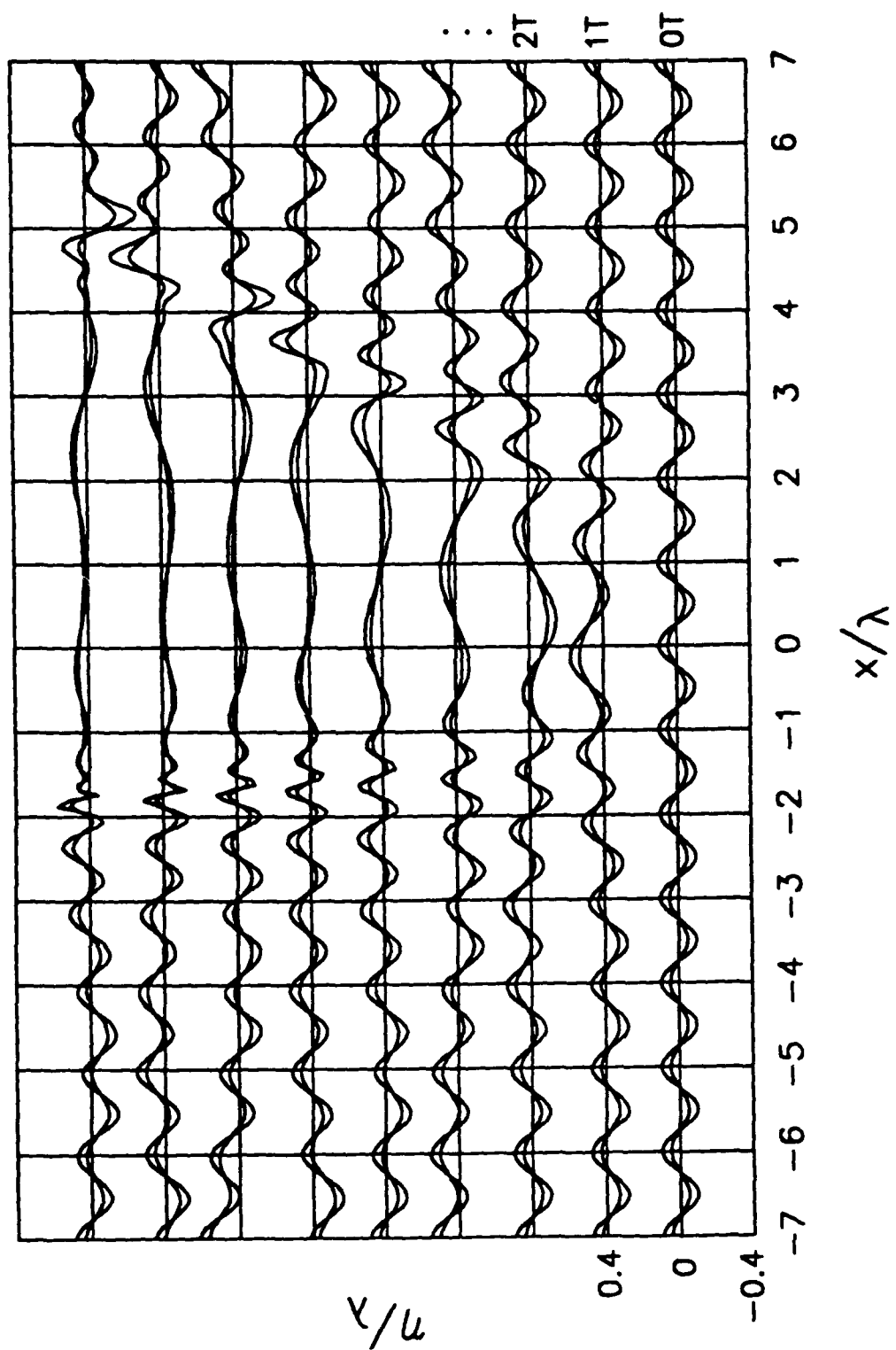Figure 32 - S/λ Variation: Vortex Paths

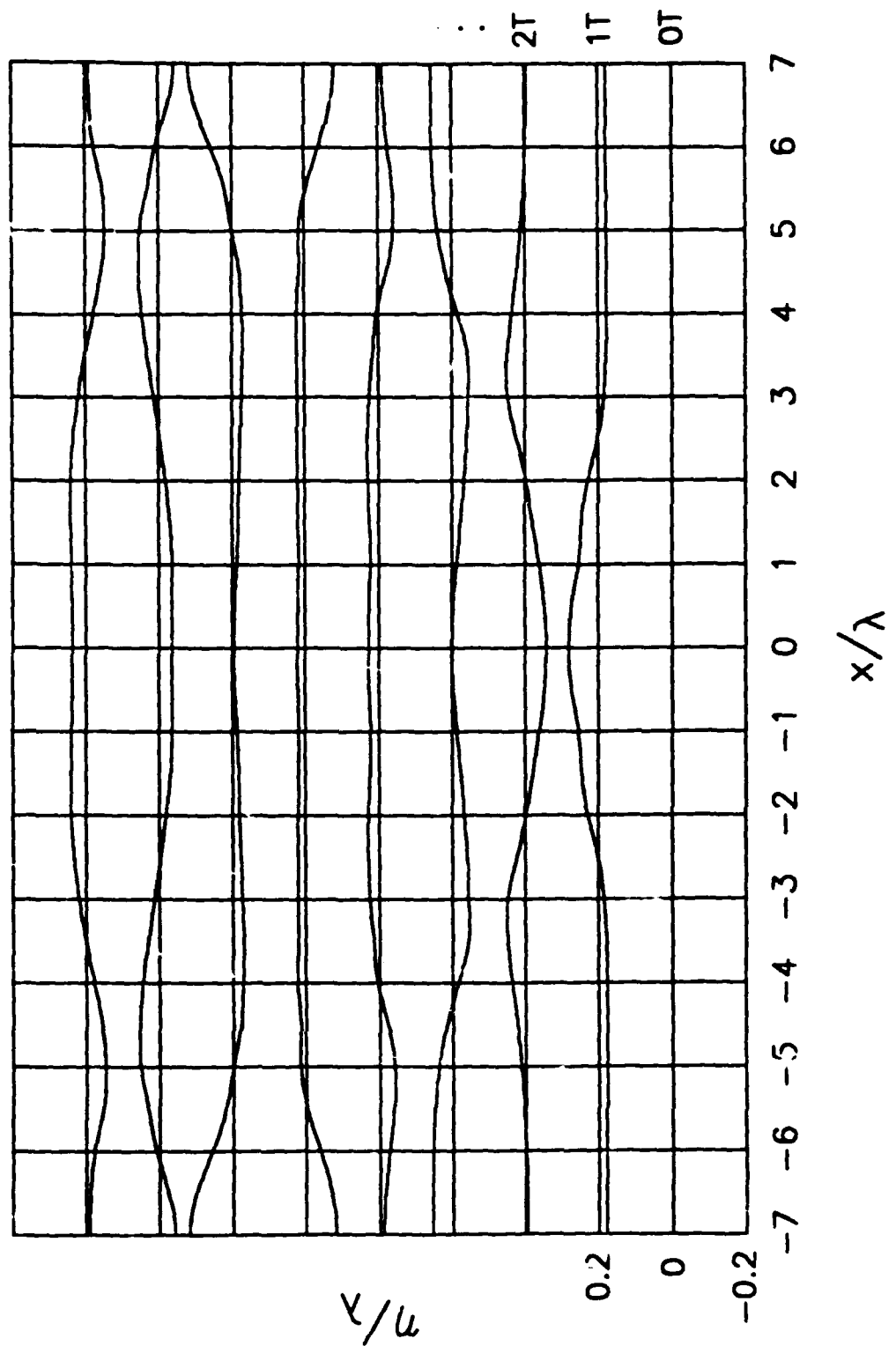Figure 33 - Ambient Wave Amplitude Variation

72

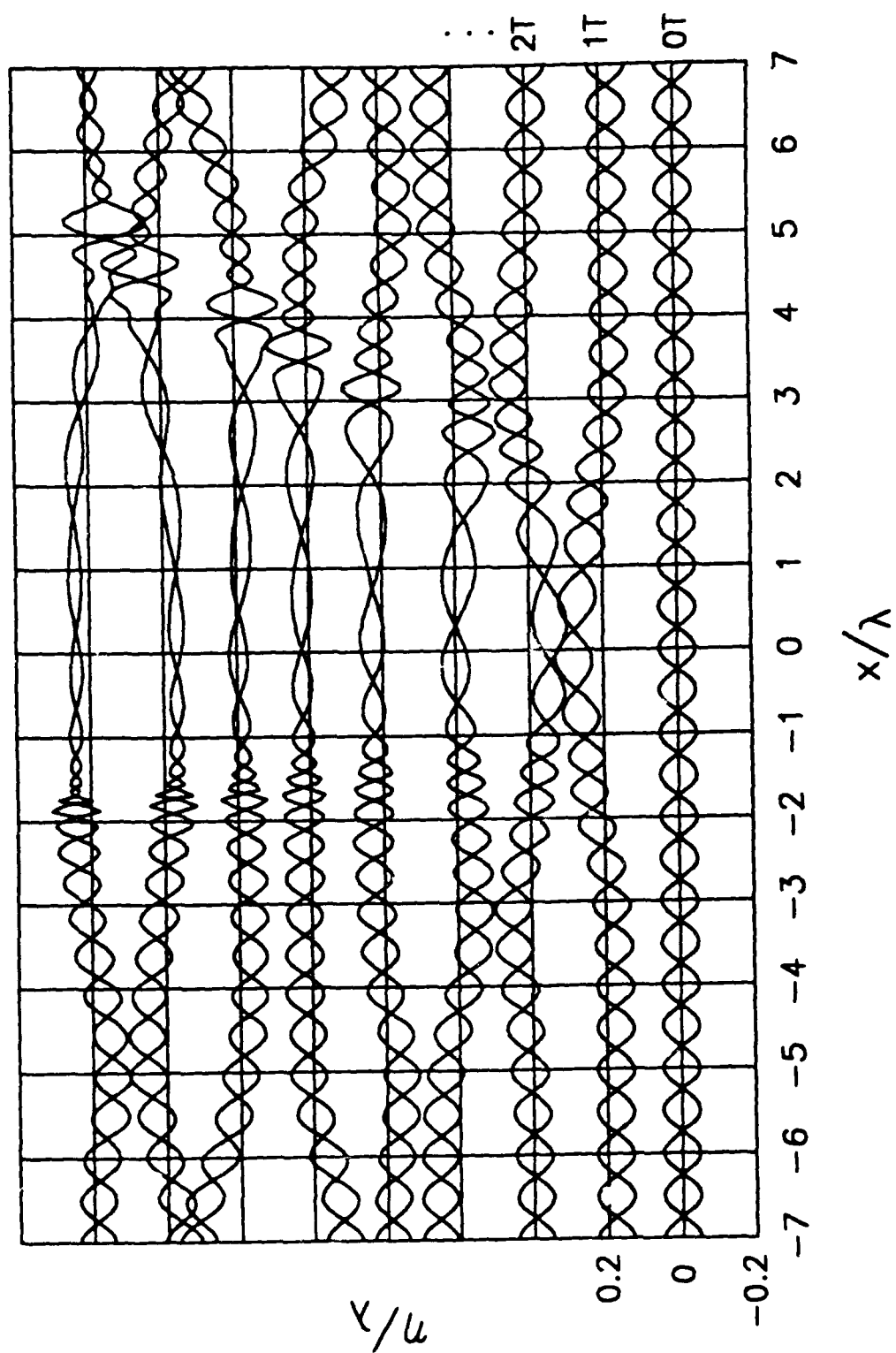Figure 34 - Residual Surface Ellivation for Amplitude Variation

Figure 35 - Ambient Wave Phase Variation

74

CHAPTER 5 - SPECTRAL ANALYSIS

In order to make the previous findings useful in the study of real ocean flows, a method of analysis must be developed which illuminates the impact of wave modification on radar images. In Chapter 1, it was shown that the reflected radar intensity is proportional to the amount of Bragg waves present in the region being illuminated by the radar. This intensity is usually expressed as the *backscattering cross section* per unit surface area, σ_0. This cross section is derived by Valenzuela (1978) in the well known Bragg scattering expression:

$$\sigma_0 = 4\pi k_r^4 \cos^4\theta \; F(\theta) \; M(2k_r \sin\theta)$$

where: k_r = radar wavenumber and θ = vertical incidence angle of radar. Here $F(\theta)$ is a scattering coefficient dependant on the radar polarization and incidence angle, and $M()$ is the component of the wave spectra corresponding to the Bragg condition. Remember, from the introduction, that the Bragg condition is satisfied when k_w (surface wavenumber component in the look direction of the radar) is equal to the argument of $M()$ in the equation above. If θ and k_w are known constants, then σ_0 is proportional to $M()$. This property indicates that a relative variation in radar backscatter over different sections of the water surface can be determined by the variations in the Bragg wave spectral component among the respective surface sections. Estimates of the relative radar intensity image can therefore be compiled by performing Finite Fourier Transforms of the surface elevation over regions corresponding in size to the resolution cell size of the radar. This will be performed here by sweeping a window across the simulated surface data and calculating the Finite Fourier Transform at various window positions. The Fourier Transform component corresponding to the Bragg waves

75

in each window position is then assigned to the midpoint location of the window. The resulting distribution of Bragg wave components over the surface is then contour plotted for comparison with SAR imagery.

5.1 METHOD

The Finite Fourier Transform used to determine the Bragg wave spectral content in a data window is given by:

$$F(k,L) = \int_{-L/2}^{L/2} f(x)\ e^{-i\ 2\pi\ k\ x}dx$$

where: L is the window width. The application of this equation to discrete data can be performed using an algorithm known as the Fast Fourier Transform, or FFT. This common method is described in detail by Bendat and Piersol.[1] The FFT output coefficients are complex in form providing phase information for each wavenumber component. Since this phase was shown to be unimportant in the previous chapter, the absolute magnitude of each wavenumber component is formed from the modulus of the real and imaginary parts:

$$M(k)=[FFT_{real}^{2}(k)\ +\ FFT_{imag.}^{2}(k)]^{1/2}$$

where: FFT(k) is an output coefficient.

Before applying the scanning FFT window to simulation results, several comments must be made here to avoid misinterpretation of the method. The regions used in computation of the spectra will be overlapped here because of the finite extent of the surface domain and the desire to have moderate sized surface patches. If the patches are allowed to be too small, the resolution of low wavenumber components decreases, resulting in undistinguishable movements of wave energy among the wavenumbers of concern. This overlapping is not

76

representative of radar imaging, and therefore the results must not be considered direct simulation of radar operation. The general trends in the resultant component levels in the Bragg wavenumber range are believed to be somewhat representative of results obtained with radar processing.

5.2 APPLICATION TO SHIP WAKE

The case examined using this technique is a simulation approximating the wake velocities from a twin screw destroyer calculated by Sween (1987). It should be noted that in simulating the full ship case, the grid resolution was lowered considerably by constraints in available computer memory. The grid density is 32 points per ambient wavelength. The ambient wavelength is set to 25 cm and corresponds to the Bragg scattering wavelength for an "L band" SAR operating at an incidence angle of 30 degrees. The initial vortex separation and depth are 5 m and 2 m, respectively. Gravitational acceleration is equal to 9.8 m/s^2, and the ambient wave amplitude is set to 2.5 cm. The vortex circulation strength, Γ, is chosen to give approximately the same maximum surface current reported by Sween (1987) for the given depth of submergence. The resulting Γ value was 1.0. The simulation domain extended to $\pm$ 6.25 m in x direction with a depth of 12.5 m. The simulation was carried out for 8 periods of the ambient wave (3.2 s) and the resultant profiles at each half period are shown in Fig 36. The corresponding downstream distance spanned by the simulation is 25 m for a ship speed of 15 knots.

The FFT window size was chosen to be 2 m wide, which is typical of SAR resolution cell dimensions. The resultant spectral resolution is 3.14/cm in

77

wavenumber giving components at wavelengths of 22 cm, 25 cm, and 28 cm.
The consecutive FFT windows were overlapped in the analysis by 3 λ. This
overlap gives denser data for examining the variations in Bragg component,
though only non-overlapping sections would be directly comparable to typical
radar imaging techniques. The Bragg component of each spectra is assigned to
the location of the FFT window center. The resulting contour plot of the
magnitude of the Bragg component versus space and time is given in Fig 37.
This plot indicates a reduction in Bragg wave component in the center region as
time progresses. In order to understand the energy flow path in this region, Fig
38 is constructed. This figure shows the progression of the spectra as the
window is traversed across the contour plot at the frame position 200. The thick
line indicates the wavenumber associated with the Bragg wavelength. Figure 38
illuminates the shift in wave energy to lower wavenumbers in the center region.
Since these wavenumber components do not satisfy the Bragg scattering criterion,
the resultant received energy at the radar is decreased. This phenomenon of
wavenumber shifting due to induced surface currents appears to produce a weaker
radar return signal in the region between the vortices. In the ocean, the wave
field can be described by the superposition of many wavelength waves. Typical
spectra from the sea (Newman[11]) indicate a decreasing level of energy as
wavenumber is increased in the range of the L Band Bragg scattering waves.
The implication of this is that though higher wavenumber (shorter) waves will be
stretched into the Bragg wavelength, thier original energy is lower. Thus one
would expect that a larger amount of energy was shifted out of the Bragg
sensitivity window than were being shifted in. The inclusion of these higher

wavenumbers would however, decrease the magnitude of variation in M() shown in Fig 37. The importance of this action is that it produces the proper trend in the surface response in the wake region of a ship and may be a significant contributor to the overall signature production process for the dark centerline wake.
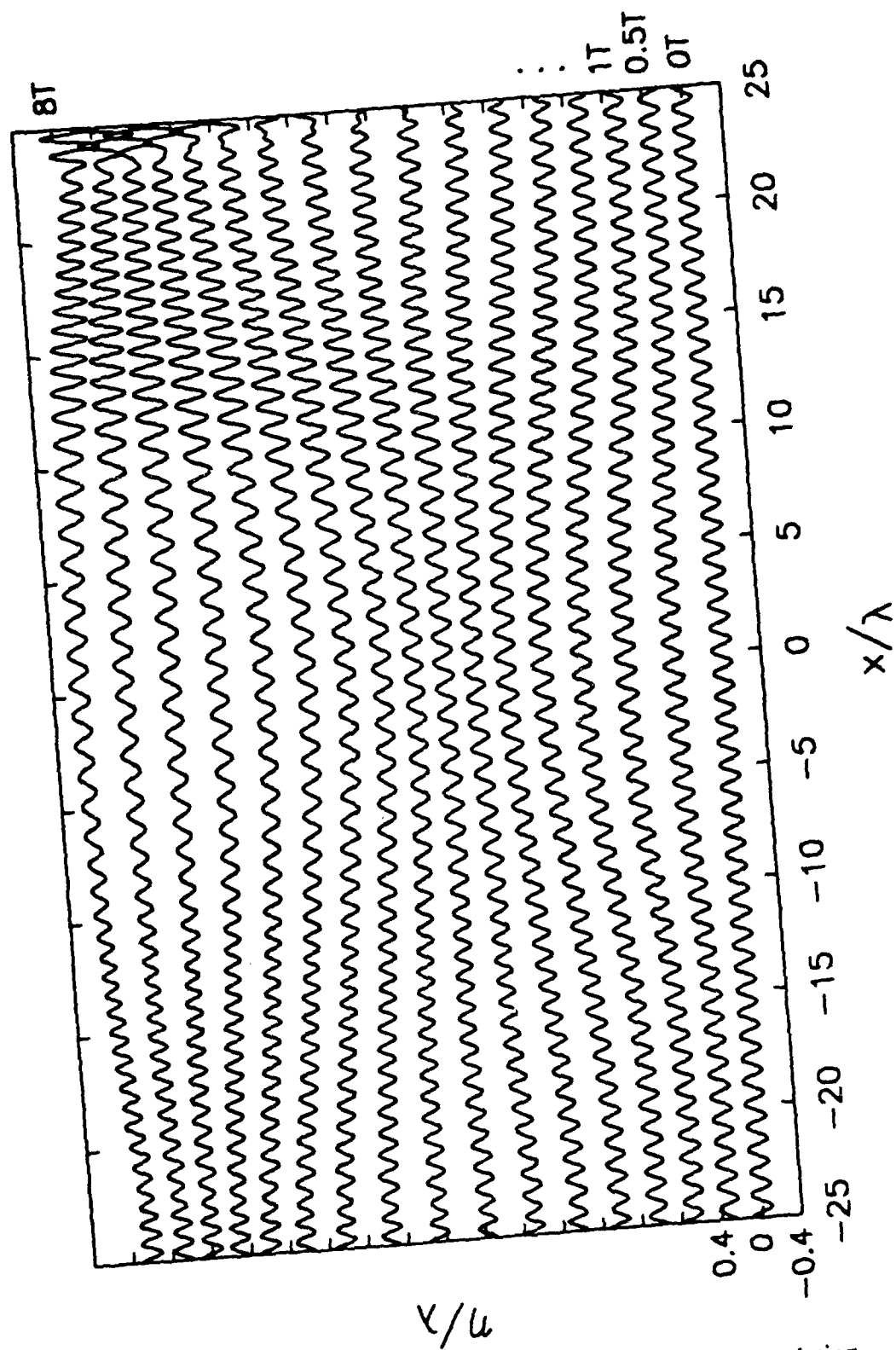
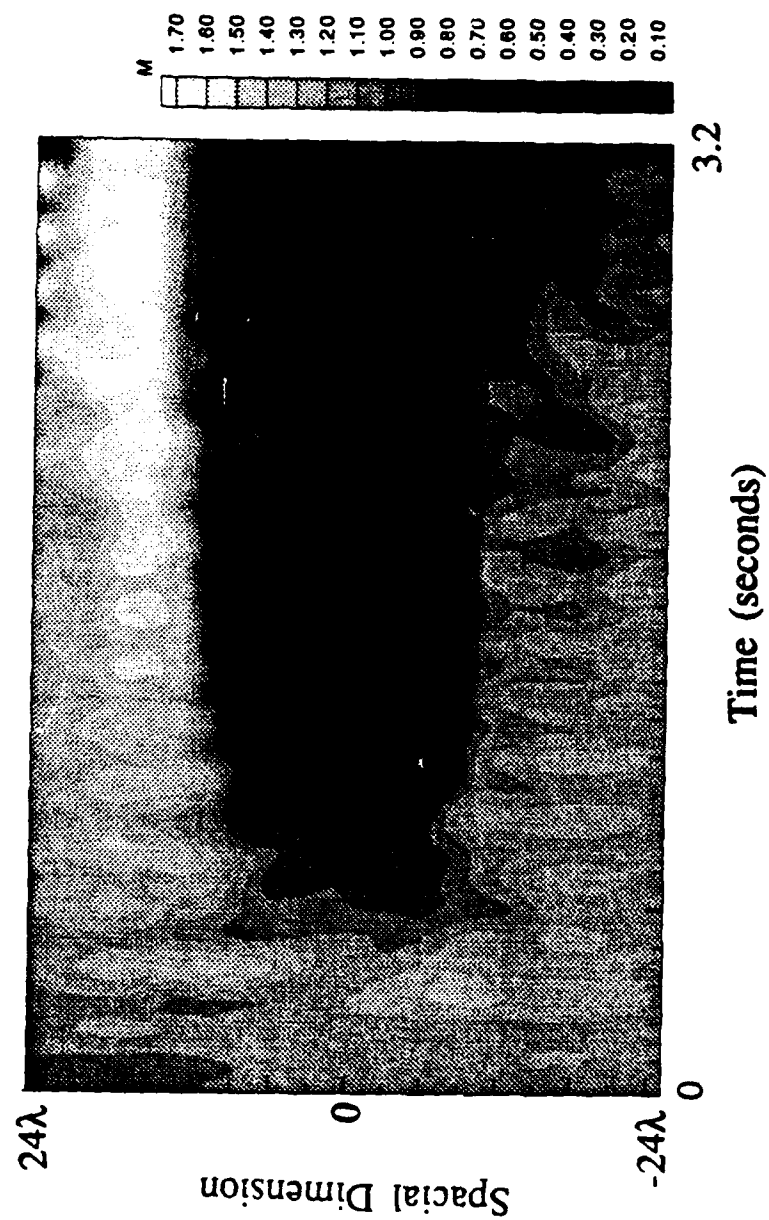Figure 36 - Free Surface Profiles For Ship Wake Simulation

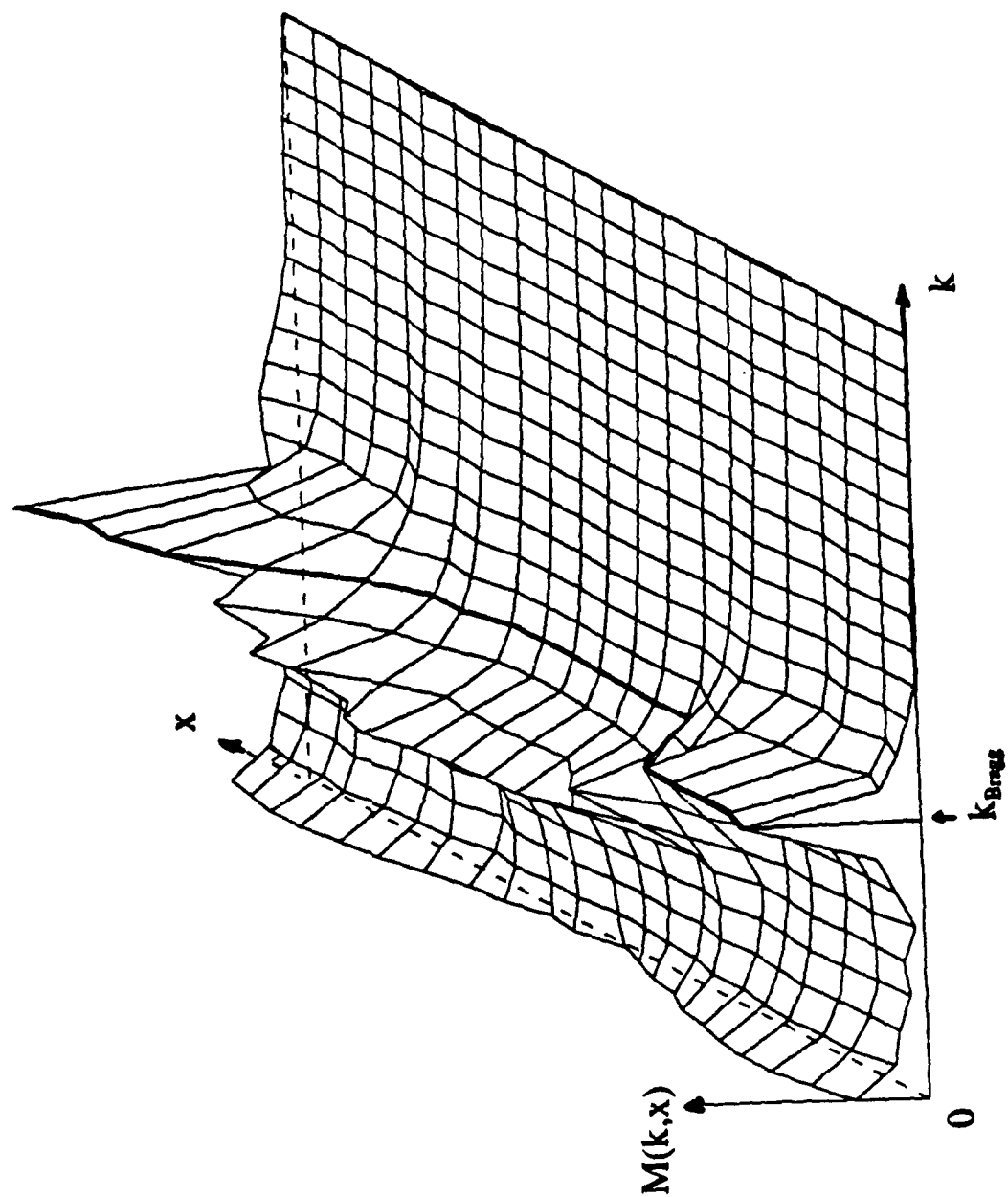Figure 37 - Ambient Wavenumber Fourier Component Space/Time Distribution

81

Figure 38 - Spectral Content in Slice of Figure 37

82

CHAPTER 6 - SUMMARY

The modification of surface waves by submerged vortices has been explored here in a straight forward progression from analytical examination through numerical simulation of a simple vortex ambient wave model. The motivation for study of this problem is the determination of ship wake impacts on synthetic aperture radar images showing dark centerline regions behind ships moving at sea. This process has lead to several discoveries in the nature of the interaction process between vortices and ambient waves.

In the initial analytical study, a new form of linearized equations was derived for the kinematic and dynamic free surface boundary conditions involving submerged vortices. The additional terms resulting from this analysis were shown to be of fundamental importance in the study of surface flows involving low Froude number vortical disturbances. Comparisons of the Alternate Linearization Method (ALM) with fully nonlinear solutions show very good agreement. Simulation results using the ALM indicate that the physical mechanism responsible for significant surface disturbances due to vortices is the vortex induced surface current. Example simulations from this program show that neglect of boundary condition terms representing the induced current give much smaller modification of surface waves than equivalent conditions with the induced surface current included.

The simulation program has also been used to examine the specific flow configuration of a vortex pair impulsively started below a free surface containing a sinusoidal ambient wave train. This examination determines which parameters

are significant in determining the form of the ambient wave modification. It is found that the Froude number of the vortices and their position relative both to each other and the free surface play the dominant roles in modifying ambient waves. The ambient wave steepness and initial relative phase with respect to the vortices have only secondary influence in the surface modification.

The simulation is then extended to represent the simple twin vortex wake model of a generic ship wake. The results of this simulation are analyzed using a scanning Fast Fourier Transform window on the surface to obtain spacial distributions of the spectral content of the surface. These spacial distributions are filtered to extract the Bragg scattering wave component and contour plotted. The resulting image shows that the shift in Bragg wave energy to longer wavelengths provides a mechanism for the observance of darker regions in centerline wake regions of ships moving in radar images.

REFERENCES

1. Bendat, J.S., and A.G. Piersol, **Random Data: Analysis and Measurement Proceedures**, Wiley Interscience, New York, pp. 252-253 and pp. 299-309, (1971).

2. Cooper, A.L. "Interactions Between Ocean Surface Waves and Currents," *NRL Mem. Rep.* 5755, (1986).

3. Fish, S., "Ambient Free Surface Wave Modification by a Submerged Vortex Pair," Ph.D. Thesis, Univ. of MD, College Park, (1989).

4. Fish, S. and J.N. Blanton, "Analysis of Propeller Wake Flow Visualization Near a Free Surface," DTRC/SHD report 1268-03, (1988).

5. Fry, D. and T.T. Huang, "Turbulent Ship Wake and Ambient Wave Interaction," *IR/IED Annual Report, DTRC* Jan. 1989, pp 27-32.

6. Griffin, O.M. and G.A. Keramidas, T.F. Sween, and H.T. Wang, "Ocean and Ship Wave Modification by a Surface Wake Flow Pattern," *NRL Mem. Rep.* 6094, (1988).

7. Lamb, H. **Hydrodynamics**, 6th Ed., Cambridge University Press, N.Y. pp. 223-224, (1945)

8. Lindenmuth, B., and D. Fry, "Viscous Macro-Wake Behind a Twin Screw High Speed Surface Ship," *DTRC SHD report* 127301, (1990).

9. Lyden, J., D. Lyzenga, R. Shuchman, and E. Kasischke, "Analysis of Narrow Ship Wakes in Georgia Strait SAR Data," *ERIM report* 155900-20-T, Ann Arbor, MI., (1985).

10. Marcus, D.L, "The Interaction Between a Pair of Counter-Rotating Vortices and a Free Surface," Ph.D. Thesis, Dept. of Mech. Eng., Univ. of Calif. at Berkeley, (1988).

11. Newman, J.N., **Marine Hydrodynamics**, MIT Press, Cambridge, MA. pp. 240-259, (1977).

12. Ohring, S. and H.J. Lugt, "Two Counter-Rotating Vortices Approaching a Free Surface in a Viscous Fluid," *DTRC report* 89/013, (1989).

13. Peltzer, R., and W. Garrett, and P. Smith, "A Remote Sensing Study of a Surface Ship Wake," *Int. J. Remote Sensing* Vol 8, no. 5, pp. 689-704, (1987).

14. Sarpkaya, T. and D.O. Henderson Jr. "Free Surface Scars and Striations Due to Trailing Vortices Generated by a Submerged Lifting Surface," *paper 85-0445 at AIAA 23rd Aero. Sci. Meeting, Jan. 14-17, Reno, Nev.* (1985).

15. Sarpkaya, T. "Trailing-Vortex Wakes on the Free Surface," *16th Symposium on Naval Hydrodynamics*, National Academy Press, pp. 38-50, (1986).

16. Sarpkaya, T., Elinsky II, J., and R. E. Leeker Jr. "Wake of a Vortex Pair on the Free Surface," *17th Symposium on Naval Hydrodynamics, Aug. 29-Sep. 2, The Hague, The Netherlands.*, (1988).

17. Simmen, J.A. and P.G. Saffman "Steady Deep-Water Waves on a Linear Shear Current," *Stud. Appl. Maths.* Vol 73, pp. 35-57, (1985).

18. Teles Da Silva, A.F. and D.H. Peregrine, "Steep Steady Surface Waves on Water of Finite Depth and Constant Vorticity," *J. Fluid Mech.* Vol 195, pp.281-302. (1988).

19. Tryggvason, G., "Deformation of a Free Surface as a Result of Vortical Flows," *Phys. Fluids* **31** (5), pp. 955, (1988).

20. Telste, J.G., "Potential Flow About Two Counter-Rotating Vortices Approaching a Free Surface," *J. Fluid Mech.* Vol 201, (1989).

21. Wehausen, J.V., and E.V. Laitone, "Surface Waves," **Handbuch der Physik IX**, Springer-Verlag, (1960).

22. Willmarth, W.W. and G. Tryggvason and A. Hirsa and D. Yu, "Vortex Pair Generation and Interaction with a Free Surface," *Phys. Fluids A*, Vol 1, Feb. 1989, pp. 170-172.

23. Wright, J.W. "Backscattering from Capillary Waves with Application to Sea Clutter," *IEEE Trans.* AP-**14**, pp. 749-754, (1966).

INITIAL DISTRIBUTION

Copies		Copies	
1	CHONR/Code 432 Rood	1	LC/Sci & Tech Div
1	NAVPGSCOL Sarpkaya	1	MARAD/Adv Ship Prog Office
2	NRL 1 Lib 1 Griffin	1	MMA/Tech Lib
		1	NASA AMES RESEARCH CTR R.T. Medan, Ms 221-2
2	NAVSEA 1 SEA 05R 1 SEA 55W3	1	NASA LANGLEY RESEARCH D. Bushnell
1	NAVFACENGCOM	1	NASA/Sci & Tech Info Facility
1	NAVOCEANO/Lib	1	NSF/Eng Div
1	NADC	1	Univ. of California, Berkeley College of Eng, NA Dept S. Berger
1	NWC		
1	NOSC	1	CA Inst of Tech A.J. Acosta
1	CEL/Code L31	1	Cornell University Grad School of Aero Eng
1	NSWC/White Oak/Lib		
1	NSWC/Dahlgren/Lib	1	Florida Atlantic Univ Ocean Eng Lib
1	NUSC NPT	1	Univ of Hawaii/Dr. Bretschneider
12	DTIC	1	Univ of Illinois/Coll of Eng J.M. Robertson Theoretical & Applied Mech
2	AFFDL/FYS 1 Dale Cooley 1 S.J. Pollock		
		1	State Univ of Iowa Iowa Inst of Hyd Research L. Landweber
1	COGARD 1 COM (E), STA 5-2		
1	Long Island Univ Grad Dept of Marine Science David Price	1	University of Maryland Eng Lib
		1	VPI J. Schetz
1	AFFDL/FDDS/J. Olsen		

Copies	
2	MIT/Dept of Ocean Eng
	1 J. Milgram
	1 J.N. Newman
4	Univ of Michigan/Dept/NAME
	1 Lib
	1 R. Beck
	1 Willmarth
	1 Trygvasson
1	Penn State Univ
	Applied Research Lab
1	SAI/Annapolis
	N. Salvesen
1	Southwest Research Inst
	Applied Mech Review
1	Stanford University
	Department of Div Eng
	Dept of Aero and Astro
	M. Van Dyke
1	Stanford Research Inst/Lib
1	Webb Institute
	Lib
1	Woods Hole, Ocean Eng Dept
1	SNAME
1	Bolt, Baranek & Newman, MA
1	Boeing Company/Aerospace Group
	R.R. Barberr
1	CALSPAN, Inc. Applied Mech Dept
1	Flow Research, Inc.
1	Eastern Research Group
2	General Dynamics Corp
	1 Convair Aerospace Div
	A.M. Cunningham, Jr. Ms 2851
	1 Electric Boat Div
	V.T. Boatwright, Jr.

Copies	
1	Gibbs & Cox, Inc.
	Tech Info Control Selection
1	Tracor Hydronautics, Inc.
	A. Goodman
1	Lockheed Aircraft Corp
	Lockheed Missiles & Space
	R.L. Waid
1	McDonnell-Douglas Corp/Douglas
	Aircraft Company -- Lib

CENTER DISTRIBUTION

Copies	Code	Name
1	012	
1	12	
1	14	Ken Nicolas
1	15	
1	152	
1	154	
1	1542	Noblesse
1	1543	
5	1543	Fish
1	1544	Reed
1	156	
1	1802	Lugt
1	1843	
1	342.1	TIC (C)
1	342.2	TIC (A)
10	3432	Reports Control